FLAgellum Member 8 modulates extravascular distribution of African trypanosomes.

Estefanía Calvo Alvarez[1*], Jean Marc Tsagmo Ngoune[1], Parul Sharma[1,2], Anneli Cooper[3], Aïssata Camara[4], Christelle Travaillé[1,5], Aline Crouzols[1], Annette MacLeod[3] and Brice Rotureau*[1,4]

[1] Trypanosome Transmission Group, Trypanosome Cell Biology Unit, INSERM U1201, Department of Parasites and Insect Vectors, Institut Pasteur, Université Paris Cité, Paris, France.

[2] Sorbonne Université, ED515 Complexité du Vivant, Paris, France

[3] Wellcome Centre for Integrative Parasitology, College of Medical, Veterinary, and Life Sciences, Henry Wellcome Building for Comparative Medical Sciences, Glasgow, Scotland, United Kingdom.

[4] Parasitology Unit, Institut Pasteur of Guinea, Conakry, Guinea.

[5] Photonic BioImaging (UTechS PBI), Institut Pasteur, Université Paris Cité, Paris, France.

*Corresponding authors:

estefania.calvo@unimi.it & brice.rotureau@pasteur.fr

Keywords: *Trypanosoma brucei*, FLAM8, flagellum, extravasation, dissemination, sensing

Short title: FLAM8 modulates extravascular trypanosome dissemination

26

27 6 Figures, 6 Supplementary Figures and 1 Supplementary Table

Abstract (231/300 words)

In the mammalian host, the biology of tissue-dwelling *Trypanosoma brucei* parasites is not completely understood, especially the mechanisms involved in their extravascular colonization. The trypanosome flagellum is an essential organelle in multiple aspects of the parasites' development. The flagellar protein termed FLAgellar Member 8 (FLAM8) acts as a docking platform for a pool of Cyclic AMP response protein 3 (CARP3) that is involved in signaling. FLAM8 exhibits a stage-specific distribution suggesting specific functions in the mammalian and vector stages of the parasite. Analyses of knockdown and knockout trypanosomes in their mammalian forms demonstrated that FLAM8 is not essential *in vitro* for survival, growth, motility and stumpy differentiation. Functional investigations in experimental infections showed that *FLAM8*-deprived trypanosomes can establish and maintain an infection in the blood circulation and differentiate into insect transmissible forms. However, quantitative bioluminescence imaging and gene expression analysis revealed that *FLAM8*-null parasites exhibit a significantly impaired dissemination in the extravascular compartment, that is restored by the addition of a single rescue copy of *FLAM8*. *In vitro* trans-endothelial migration assays revealed significant defects in trypanosomes lacking *FLAM8*. FLAM8 is the first flagellar component shown to modulate *T. brucei* distribution in the host tissues, possibly through sensing functions, contributing to the maintenance of extravascular parasite populations in mammalian anatomical niches, especially in the skin.

Author Summary (192/200 words)

Trypanosoma brucei parasites cause neglected tropical diseases termed human and animal African trypanosomiases. Transmitted by the bite of an infected tsetse fly, upon deposition in the skin of a mammalian host, these parasites occupy both the vasculature and extravascular tissues. Currently, the biology of tissue-resident parasites is not well understood, and the parasite factors that mediate extravascular colonization are not known. Using quantitative *in vivo* bioluminescence imaging and *ex vivo* gene expression quantification in host infected tissues and blood, we reveal that the flagellar parasite protein FLAM8 modulates the extravascular dissemination of trypanosomes in the mammalian host. FLAM8 is known to act as a docking platform for signaling complexes in the flagellum, but we observe that it does not influence parasite differentiation into transmissible stages. However, we show that the absence of FLAM8 results in the loss of a key component of the flagellar adenylate cyclase signaling complexes, and reduces parasite migration through endothelial cell monolayers, suggesting that FLAM8 is important for parasite exchanges between the intravascular and the extravascular compartments. This work identifies a key trypanosome flagellar component involved in host-parasite interactions, including the modulation of parasite tropism and extravascular dissemination.

67 **Introduction**

68 *Trypanosoma brucei* is an extracellular parasite responsible for African
69 trypanosomiases, including sleeping sickness in humans and *nagana* in cattle. African
70 trypanosomes are blood and tissue-dwelling protists transmitted by the bite of the
71 blood-feeding tsetse fly (*Glossina* genus). In the mammalian host, parasites face
72 different micro-environments, including deadly challenges by multiple types of host
73 immune responses and variable availability of carbon sources. This requires major
74 morphological and metabolic adaptations, driven by the activation of specific gene
75 expression programs, that are critical for life-cycle progression [1-3]. Recently, the
76 importance of extravascular tropism for *T. brucei* has been re-discovered in animal
77 models: in addition to the brain, parasites occupy most mammalian tissues, especially
78 the skin and the adipose tissues [4-7]. However, the role of extravasation and
79 sequestration of trypanosomes in specific anatomical niches and the underlying
80 molecular processes are not understood yet.

81 The trypanosome flagellum is an essential organelle anchored along the surface of the
82 cell body and present in all stages of its development [8]. It is essential for parasite
83 viability [9], cell division and morphogenesis [10], attachment to the tsetse salivary
84 glands [11] and motility [12]. In the insect host, the flagellum remains at the forefront
85 of the cell and is likely to be involved in sensory and signaling functions required for
86 host-parasite interactions [13, 14]. In the mammalian host, flagellar motility was shown
87 to be critical for establishment and maintenance of bloodstream infection [15].
88 Nevertheless, the contributions of the trypanosome flagellum to parasite tropism and
89 spatiotemporal dissemination outside vessels in the mammalian host remained to be
90 explored.

91 A proteomic analysis of intact flagella purified from the insect stage of the parasite
92 identified a group of flagellar membrane and matrix proteins with unique patterns and
93 dynamics [16]. Amongst them, one large protein (3,075 amino acids) termed FLAgellar
94 Member 8 (FLAM8) is present only at the distal tip of the flagellum in the insect
95 procyclic form [16-18]. Interestingly, FLAM8 is redistributed along the entire length of
96 the flagellum in mammalian forms, including in stumpy transmissible stages [19], which
97 may imply a stage-specific function for this protein. Therefore, we hypothesized that
98 FLAM8 could be involved in host-parasite interactions or in developmental
99 morphogenesis. Here, we investigated the roles of FLAM8 in mammalian form
100 parasites *in vitro* in terms of survival, proliferation, motility, and differentiation, as well
101 as the *in vivo* dynamics of the intravascular and extravascular parasite burden over
102 the course of murine infection. Intriguingly, experimental infections in mice monitored
103 and quantified by bioluminescence imaging and gene expression analyses
104 demonstrated the involvement of FLAM8 in parasite dissemination in the extravascular
105 compartments. In addition, *in vitro* transmigration studies detected impaired
106 extravasation ability of *FLAM8*-deprived parasites, possibly resulting from the loss of
107 components of flagellar adenylate cyclase signaling complexes.

108 **Results**

109 ***FLAM8* RNAi silencing does not affect parasite survival**

110 The differential distribution of FLAM8 in the flagellum of the different trypanosome
111 stages [19] raises the question of its specific functions during the parasite life cycle. To
112 investigate the potential role(s) of FLAM8 in the mammalian host, bloodstream form
113 parasites were first engineered for inducible RNAi knockdown of *FLAM8* in a
114 monomorphic strain expressing a mNeonGreen-tagged version of FLAM8. In order to
115 monitor their behavior in mouse by whole-body imaging approaches, these
116 *FLAM8::mNG FLAM8*^{RNAi} mutants were subsequently transformed to overexpress a
117 chimeric triple reporter protein [20]. Upon RNAi induction with tetracycline for 72 h *in*
118 *vitro*, *FLAM8* expression was reduced by 60% at the mRNA level (Fig. 1A) and became
119 undetectable at the protein level by immunofluorescence (Fig. 1B). Parasite growth
120 was monitored over 6 days upon induction of RNAi and no impact on proliferation was
121 observed (Fig. 1C), which suggests that FLAM8 is possibly not essential for survival of
122 mammalian forms of the parasite in cell culture conditions.

123 Then, the linear correlation between the emitted bioluminescence and the number of
124 parasites was assessed in an IVIS Spectrum imager prior to *in vivo* challenge (Fig.
125 S1). To get insights into the function of FLAM8 in the mammalian host, groups of male
126 BALB/c mice were infected by the intraperitoneal route with 10^5 parasites of the
127 parental, non-induced and induced cell lines (Fig. 1D). *In vivo* RNAi silencing of *FLAM8*
128 was maintained in mice by the addition of doxycycline in sugared drinking water 48 h
129 prior infection and until the end of the experiment. The course of the infection was
130 monitored daily by i) quantifying the parasitemia, and ii) acquiring the bioluminescent
131 signal emitted by the parasites in the entire organism with an IVIS Spectrum imager.
132 The number of parasites in the extravascular compartment at a given timepoint can be

133 extrapolated by subtracting the known number of trypanosomes in the vascular system
134 (parasitemia x blood volume, according to body weight) from the total number of
135 parasites in the organism (total bioluminescence). No differences were detected,
136 neither in the establishment of the infection and the subsequent variations in the
137 number of intravascular parasites (Fig. 1E, IV), nor in the number of parasites
138 occupying extravascular tissues (Fig. 1F, EV). Similar population profiles were
139 observed over the course of the infection for both intra- and extravascular parasites in
140 each of the three independent groups of infected mice (Fig. 1D-F). In the extravascular
141 compartment, no significant differences were detected in terms of parasite
142 dissemination over the entire animal body in any group (Fig. 1G).

143 ***FLAM8* knockout does not affect trypanosome growth *in vitro***

144 Considering that i) *FLAM8* RNAi silencing efficiency was only partial (40% *FLAM8*
145 mRNA left after 72 h of induction), ii) the efficacy of doxycycline-induced *FLAM8*
146 repression could have been even lower *in vivo*, and that iii) the parental strain used for
147 this first strategy was monomorphic (i.e. unable to differentiate into tsetse adapted
148 stumpy stages), we reasoned that a gene knockout approach in a pleomorphic strain
149 would be more appropriate to evaluate the potential role(s) of FLAM8 during the
150 mammalian host infection. Therefore, a Δ*FLAM8* knockout cell line was generated in
151 pleomorphic trypanosomes by homologous recombination. The full replacement of one
152 *FLAM8* allele and the partial replacement of the second one (to allow the use of a
153 shorter *in situ* rescue sequence than the long *FLAM8* coding sequence) by distinct
154 resistance cassettes was verified by whole-genome sequencing and PCR (Fig. S2).
155 The absence of full or truncated FLAM8 protein expression was further assessed by
156 quantitative immunofluorescence analysis with an anti-FLAM8 antibody [19] targeting
157 the region of FLAM8 that was not replaced in the second allele (Fig. 2A). This was also

158 confirmed at the mRNA level by RT-qPCR (Table S1). The trypanosome cell lines
159 generated were further transformed to express the chimeric triple reporter construct
160 [20], and the linear correlation between the bioluminescence signal and the total
161 number of parasites was analyzed for all strains both *in vitro* and *in vivo* (Fig. S3). In
162 Δ*FLAM8* knockout parasites where a rescue copy of one *FLAM8* allele was added
163 back into its endogenous locus, the FLAM8 distribution was restored along most of the
164 flagellum length, as assessed by immunofluorescence analysis (Fig. 2A). This was
165 confirmed by quantifying the total fluorescence intensities of the FLAM8 signal along
166 the full flagellum length in all parasite strains (Fig. 2B): a background fluorescence
167 signal was detected in knockout trypanosomes, while the rescue cell line presented an
168 intermediate level of FLAM8 expression. No impact on parasite growth in culture
169 conditions was observed (Fig. 2C). Next, we investigated whether the loss of FLAM8
170 could have impacted the total length of the flagellum based on the measurement of the
171 signal obtained with the axonemal marker mAb25: no difference was observed among
172 BSF lines (Fig. 2D). In addition, the absence of *FLAM8* did not affect parasite speed
173 or linearity *in vitro*, neither in 0.5% methylcellulose liquid medium (Fig. 2E-F) nor in
174 1.1% methylcellulose viscous medium (Fig. 2G-H). Compatible with our previous
175 observations after RNAi silencing, these results show that pleomorphic trypanosomes
176 tolerated the loss of *FLAM8 in vitro*.

177 ***FLAM8* knockout affects trypanosome distribution in the mammalian host**

178 Then, functional investigations in the mammalian host were performed by infecting
179 BALB/c mice either with the pleomorphic parental strain, three distinct Δ*FLAM8*
180 knockout subclones (resulting from independent recombination events) or one
181 Δ*FLAM8* strain bearing a rescue copy of *FLAM8* (Fig. 3 and S4). The infections were
182 monitored daily for 4 weeks by quantifying the parasitemia and the bioluminescence

183 signals emitted from whole animals (Fig. 3A). Null mutant parasites were able to
184 establish an infection in the bloodstream as well as in the extravascular compartment.
185 Within the vasculature, the overall amounts of parasites throughout the whole
186 experimental infection were slightly higher in mice infected with the three Δ*FLAM8*
187 subclones as compared to mice infected with the parental strain, except between days
188 5 and 12 with a lower and variable parasitemia observed just after the first peak of
189 parasitemia (Fig. 3B and D). On the other hand, quantitative analyses of extravascular
190 parasites showed a different scenario. Unlike in the intravascular compartment,
191 significantly lower numbers of extravascular trypanosomes were observed between
192 day 5 to 12, and from day 19 post-infection until the end of the experiment at day 27,
193 evidencing an impaired extravascular colonization for Δ*FLAM8* parasites as compared
194 to parental controls (Fig. 3C and E). To note, distribution profiles of all pleomorphic
195 strains were different from those observed in mice infected with monomorphic
196 parasites: larger amounts of trypanosomes were seen occupying the extravascular
197 compartment reaching up to 5-8x10^9 parasites, while the maximum amount found in
198 the bloodstream never exceeded 7x10^7 trypanosomes (Fig. 3C and B, respectively).
199 Furthermore, quantification of the parasite spreading over the whole animal bodies
200 showed that the depletion of *FLAM8* resulted in significantly impaired dissemination of
201 Δ*FLAM8* null mutant parasites in the extravascular compartment (days 5 to 14, 19 and
202 27 post-infection). This was mostly restored in trypanosomes bearing a rescue copy of
203 *FLAM8* (Fig. 3F).

204 ***FLAM8* knockout impairs extravascular trypanosome dissemination**

205 We reasoned that the accuracy of the intra- Vs. extravascular parasite population
206 estimation from bioluminescence detection on small regions of interest could be
207 limited. Therefore, the same experiment was repeated, with a lower time resolution,

208 yet with comparable trends in terms of extravascular parasite populations and parasite
209 dissemination according to the strain (Fig. 4A-C and S5). At the end of this second
210 experimental challenge (Day 24), most trypanosomes were removed from the vascular
211 system by saline perfusion prior to organ dissection. Individual organs were then
212 collected for quantifying the expression of different parasite genes by RT-qPCR. The
213 total number of parasites in each sample was calculated per mg of tissues by using a
214 *Tubulin* RT-qPCR standard curve. To better compare the variations of the parasite
215 populations in each compartment between strains, the Delta number of parasites was
216 calculated as the difference between the number of parasites in each tissue sample of
217 a given mouse and the number of parasites in the blood sample from the same mouse.
218 First, the absence of *FLAM8* transcripts was confirmed in animals infected with
219 Δ*FLAM8* parasites, whereas FLAM8 mRNAs were detected in mice infected with both
220 the parental and rescue strains (Table S1). Normalized *Tubulin* expression was then
221 used to compare the parasite densities between organs and strains (Fig. 4D-E and
222 S6). In all mice, the highest number of extravascular parasites was observed in the
223 skin. In all organs, a marked decrease in the number extravascular parasites was
224 detected from mice infected with Δ*FLAM8* parasites as compared to mice infected by
225 parental and rescue parasites (Fig. 4D and S6). When considering the average
226 difference between the number of parasites in organs versus blood by strains, the
227 statistically significant decrease in extravascular *FLAM8*-deprived parasite densities
228 appeared even more clearly (Fig. 4E). The rescue cell line recapitulated EV parasite
229 profiles in all organs examined with an average Delta number of parasites that was not
230 statistically different from that of the parental line.
231 We reasoned that this reduced extravascular dissemination of *FLAM8*-deprived
232 parasites could possibly be due to: (1) a lower proliferation rate, (2) a defect in motility,

233 (3) a higher rate of differentiation into non-proliferative stumpy forms, and / or (4) an
234 extravasation defect. The two first hypotheses could immediately be discarded as no
235 difference was observed between strains, neither in cell growth *in vitro* (Fig. 2C) and
236 *in vivo* (Fig. 3B and 4A), nor in cell motility *in vitro* (Fig. 2E-H). The two last hypotheses
237 were then successively tested.

238 **The absence of FLAM8 does not affect parasite differentiation**

239 The systemic reduction in the extravascular Δ*FLAM8* parasite population could result
240 from a disequilibrium in the parasite differentiation into non-proliferative transmissible
241 forms. Therefore, we assessed whether the absence of FLAM8 could have impacted
242 the differentiation of proliferative slender into transmissible stumpy forms in the blood
243 and organs by immunofluorescence or RT-qPCR. In cultured parasites, the absence
244 of *FLAM8* did not significantly alter differentiation (Fig. 5A-B), and freshly differentiated
245 *FLAM8*-deprived stumpy parasites were able to further differentiate and maintain *in*
246 *vitro* as procyclic trypanosomes, as were the parental and rescue strains (Fig. 5C-D).
247 *In vivo*, the natural differentiation of proliferative slender into non-proliferative stumpy
248 parasites was confirmed by RT-qPCR on blood and dissected organs at the end of the
249 experiment (Fig. 5E, Day 24 of the second *in vivo* challenge). For each sample, *Tubulin*
250 expression was used to normalize the *PAD1* mRNA levels to compare the average
251 levels of parasites expressing *PAD1* mRNAs over the total parasite populations
252 between organs and strains (Fig. 5E), with a higher Delta CqPAD1-CqTub correlating
253 with a lower amount of *PAD1* transcripts in the organ. *PAD1* transcripts were detected
254 in each organ at least in one individual, showing that all tested organs represent a
255 suitable environment for the parasites to differentiate into transmissible forms (Table
256 S1). In mice infected with the parental and rescue strains, the highest levels of *PAD1*
257 transcripts were detected in blood and skin, suggesting an accumulation or an

258 increased rate of differentiation in organs directly involved in parasite transmission
259 (Table S1). No *PAD1* transcripts were detected in the gut, liver and spleen in mice
260 infected with the parental and rescue strains, whereas *PAD1* transcripts were detected
261 in these three organs from mice infected with the Δ*FLAM8* strains. However, when
262 considering the average Delta CqPAD1-CqTub in the entire organisms by strains, the
263 relative proportions of parasites expressing *PAD1* mRNAs were not significantly
264 different among groups, confirming that FLAM8 is not involved in parasite
265 differentiation (Fig. 5E). In addition, an anti-PAD1 immunofluorescence staining of
266 blood smears sampled at the first peak of parasitemia visually confirmed the presence
267 of differentiated stumpy parasites in all infected animal groups (Fig. 5F, Day 5 of the
268 first *in vivo* challenge).

269 **Parasite extravasation is impaired in *FLAM8*-deprived trypanosomes**

270 To test the last hypothesis, we asked whether the absence of FLAM8 might influence
271 the way parasites traverse the vessel walls to access extravascular tissues. We first
272 established a transmigration assay using human umbilical vein endothelial cells
273 (HUVECs) grown to confluence on polyester transwell inserts with 3 µM pores,
274 separating two chambers to mimic the vascular endothelium *in vitro* (Fig. 6A). Once
275 HUVECs have reached confluence, 10^6 parental, *FLAM8*-deprived or rescue
276 trypanosomes were added to the upper chamber and incubated for 24h. The number
277 of trypanosomes that migrated through the endothelial monolayer into the lower
278 chamber and the number of non-migrating trypanosomes remaining in the upper
279 chamber of the transwell system were counted by flow cytometry to determine the
280 transmigration percentage. Interestingly, all *FLAM8*-knockout subclones showed a
281 significant reduction in transmigration relative to parental controls (25,6%, 70,7% and
282 33,8% of parasites crossing for KO1, 2 and 3, respectively) (Fig. 6B). Rescue

283 trypanosomes expressing only one *FLAM8* allele exhibited an intermediate
284 transmigration phenotype in which 59,2% of the parasites migrated through the
285 endothelial monolayer (Fig. 6B), which was lower than for parental trypanosomes but
286 significantly higher than for KO1 and KO3 null mutants (Fig. 6B). This demonstrates a
287 strong impairment of parasites lacking *FLAM8* to cross through a confluent layer of
288 endothelial cells, which was partially restored in rescue parasites.
289 Knowing that, in mammalian forms, FLAM8 was recently identified to be part of a
290 flagellar complex including the cyclic AMP response protein 3 (CARP3) [21], we
291 reasoned that this trans-endothelial crossing impairment could be caused by a defect
292 in sensing and / or signaling. To assess how the absence of FLAM8 was impacting
293 CARP3 localization and/or abundance, CARP3 distribution was investigated by
294 quantitative immunofluorescence in all strains upon methanol fixation (Fig. 6C-D). As
295 expected, CARP3 was detected along the entire flagellum length in parental
296 mammalian forms, but not in Δ*FLAM8* parasites where the fluorescent signal was
297 weaker and restricted to the distal part of the flagellum (Fig. 6C-D). This demonstrates
298 the presence of at least two distinct pools of CARP3, one being independent of FLAM8
299 for its localization to the anterior part of the flagellum. The presence of a *FLAM8* rescue
300 copy in Δ*FLAM8* parasites restored the detection of CARP3 along the entire flagellum,
301 yet in lower amounts than in parental cells (Fig. 6C-D).
302
303 In total, these data show that FLAM8 is likely involved in a cellular pathway modulating
304 trypanosome extravasation and consequently trypanosome dissemination in the
305 extravascular compartment of the mammalian host.

306 **Discussion**

307 The differential localization of FLAM8 from the very distal tip in tsetse midgut procyclic
308 parasites to the entire flagellum length in the mammalian-infectious stages [19]
309 prompted us to speculate that FLAM8 could play a distinct and specific role in each
310 host. Here, we present for the first time the connection of a flagellar protein with the
311 efficiency of trypanosomes to disseminate outside the mammalian host vasculature,
312 especially in the skin. Quantitative analyses of experimental animal infections
313 monitored by bioluminescence imaging and gene expression analysis showed that the
314 absence of FLAM8 impairs parasite extravasation and dissemination in the host
315 extravascular compartment over the time of the infection, which was mostly recovered
316 by the integration of a single rescue copy of the *FLAM8* gene in the endogenous locus.

317 **1. FLAM8 and trypanosome transmission**

318 In the bloodstream, the balance between proliferative slender parasites and tsetse-
319 adapted stumpy forms responds to a quorum sensing mechanism involving the
320 production of oligopeptides and their reception through a specific transporter [22]. The
321 absence of FLAM8 did not alter the ability of the parasites to differentiate into
322 transmissible stumpy forms at the two observed time points (first peak of parasitemia
323 and 3 weeks after infection). Although stumpy proportions were not evaluated over the
324 entire course of the infection, this evidence suggests that FLAM8 does not play an
325 integral role in this process. In addition, the retained ability of *FLAM8*-deprived stumpy
326 cells to differentiate into procyclic forms *in vitro* suggests that they could further pursue
327 their cyclical development upon ingestion by a tsetse fly.

328 Extravascular trypanosomes occupy the interstitial space of several organs, including
329 the central nervous system, testes, adipose tissues, and skin [4-7, 23-25]. The
330 relevance of skin-dwelling trypanosomes in parasite transmission has been

331 demonstrated by xenodiagnosis experiments, early after the infective bite [26], or later
332 in the infection [4], even in the absence of detectable parasitemia. More recently, the
333 presence of extravascular trypanosomes was confirmed in the skin of confirmed and
334 suspected cases of sleeping sickness [27]. Here, we show that all tested organs
335 represent a suitable environment for the parasites to differentiate into transmissible
336 forms, yet the highest amounts of *PAD1* transcripts were detected in blood and skin,
337 suggesting an increased rate of differentiation, or an accumulation of differentiated
338 stumpy forms in organs directly involved in parasite transmission. In total, the impaired
339 spreading of *FLAM8*-null parasites over the extravascular compartment would
340 mathematically reduce the probability for parasites to be ingested by tsetse flies. This
341 could be especially significant for the skin, that has the highest parasite density, and
342 the highest overall parasite load due to its size, at the direct interface with insect
343 vectors.

344 **2. On the possible cellular function(s) of FLAM8**

345 Proliferative slender trypanosomes are highly mobile [28] and this motility was proved
346 to influence virulence *in vivo*. For instance, the lack of propulsive motility in flagellar
347 dynein light chain 1 (*LC1*) knockout mutants resulted in the inability of trypanosomes
348 to establish an infection in the bloodstream [15]. Here, *FLAM8* depletion in pleomorphic
349 mammalian forms did not alter parasite growth and cell motility neither in liquid
350 medium, nor in matrix-containing medium with a viscosity closer to the parasite micro-
351 environment *in vivo*. However, quantitative analyses showed that *FLAM8*-null
352 trypanosomes were less numerous in extravascular tissues as compared to parental
353 controls. Assuming that parasite motility could be different in tissues and interstitial
354 spaces with biophysical properties distinct from those in the blood [28, 29], one cannot
355 exclude that the motility of Δ*FLAM8* knockout parasites might be somehow altered in

356 the extravascular compartment. Intravital imaging for motility analyses at the cell level
357 would be needed to confirm this hypothesis.
358 Historically, most studies on *T. brucei* virulence in experimental infections have
359 considered the blood circulation almost as the sole host compartment parasitized by
360 trypanosomes, whereas extravascular parasite niches and the underlying exchanges
361 between both compartments have been underestimated for long. De Niz and
362 colleagues recently identified adhesion molecules as key players for tissue tropism
363 [30]. They showed that reservoir establishment happens before vascular permeability
364 is compromised, suggesting that extravasation is an active mechanism, and depends
365 on trypanosome interactions with endothelial surface adhesion molecules, such as E-
366 selectin, P-selectins, or ICAM2 [30]. Here, we showed that the absence of FLAM8 led
367 to a strong impairment in parasite extravasation. The fact that *FLAM8*-null
368 trypanosomes were not able to disseminate properly over the extravascular
369 compartment could somehow possibly imply defects in the way parasites sense their
370 microenvironment or interact with the host endothelial cells, resulting in an alteration
371 of their extravascular tropism.
372 The insect forms´ coordinated social motility *in vitro* is linked to cAMP signaling at the
373 flagellar tip [31, 32], i. e. where FLAM8 localizes [19]. The architecture of an adenylate
374 cyclase complex in the tip nanodomain was recently shown to be essential for social
375 motility and salivary gland colonization [21]. In this complex, CARP3 interacts with the
376 catalytic domain of adenylate cyclases and regulates abundance of multiple adenylate
377 cyclase isoforms. We recently demonstrated that the CARP3 tip localization depends
378 on the presence of FLAM8 acting as a scaffold protein [21]. Thus, trypanosome
379 migration and transmission in the tsetse vector specifically depend on adenylate
380 cyclase complex-mediated signaling in the tip nanodomain including FLAM8 [21].

381 Interestingly, we have recently shown that CARP3 and FLAM8 are both redistributed
382 along the entire length of the flagellum during their differentiation to the mammalian
383 stage, and that they further remain associated in flagellar complexes in mammalian
384 forms [21]. Here, this was confirmed by the significant decrease of the pool of CARP3
385 detected in the proximal flagellum region of *FLAM8*-deprived parasites. Altogether,
386 these data could reflect a possible specific function of some CARP3-containing
387 signaling complexes depending on FLAM8 for their sub-flagellar localization.
388 Environmental sensing and / or signaling, possibly through direct contact with host cell
389 receptors may play a role in extravasation. We hypothesize that the absence of FLAM8
390 would destabilize or delocalize these signaling complexes, impairing parasite sensing,
391 signaling and / or adhesion functions, hence preventing the parasite to efficiently cross
392 vascular endothelia.
393
394 To our knowledge, FLAM8 is the first flagellar component affecting parasite
395 extravasation and their subsequent dissemination in the extravascular host tissues *in*
396 *vivo*. Further investigations on the FLAM8 interactions with other possible partners in
397 the flagellum would help to unravel the roles of this fascinating and essential organelle,
398 especially regarding the modulation of trypanosome tropism, extravasation and
399 spreading in their mammalian hosts, and its implications in parasite virulence and
400 transmission.

401 **Materials and Methods**

402 **Strains, culture and *in vitro* differentiation**

403 The AnTat 1.1E Paris pleomorphic clone of *Trypanosoma brucei brucei* was derived
404 from a strain originally isolated from a bushbuck in Uganda in 1966 [33]. The
405 monomorphic *T. brucei* strain Lister 427 [34] was also used. All bloodstream forms
406 (BSF) were cultivated in HMI-11 medium supplemented with 10% (v/v) fetal bovine
407 serum (FBS) [35] at 37°C in 5% CO_2. For *in vitro* slender to stumpy BSF differentiation,
408 we used 8-pCPT-2′-O-Me-5′-AMP, a nucleotide analog of 5'-AMP from BIOLOG Life
409 Science Institute (Germany). Briefly, $2x10^6$ cultured pleomorphic AnTat 1.1E slender
410 forms were incubated with 8-pCPT-2′-O-Me-5′-AMP (5 µM) for 48 h [36]. For specific
411 experiments, *in vitro* differentiation of BSF into procyclic forms was performed by
412 transferring freshly differentiated short stumpy forms into SDM-79 medium
413 supplemented with 10% (v/v) FBS, 6 mM cis-aconitate and 20 mM glycerol at 27°C
414 [37].

415 Monomorphic BSF "Single Marker" (SM) trypanosomes are derivatives of the Lister
416 427 strain, antigenic type MITat 1.2, clone 221a [38], and express the T7 RNA
417 polymerase and tetracycline repressor. *FLAM8*^{RNAi} cells express complementary
418 single-stranded RNA corresponding to a fragment of the *FLAM8* gene from two
419 tetracycline-inducible T7 promoters facing each other in the pZJM vector [39]
420 integrated in the rDNA locus [40]. Addition of tetracycline (1 µg/mL) to the medium
421 induces expression of sense and anti-sense RNA strands that can anneal to form
422 double-stranded RNA (dsRNA) and trigger RNAi. For *in vivo* RNAi studies in mice,
423 doxycycline hyclate (Sigma Aldrich) was added in sugared drinking water (0.2 g/L
424 doxycycline hyclate combined with 50 g/L sucrose).

425 **Generation of FLAM8 RNAi mutants**

426 For the generation of the *FLAM8*^{RNAi} cell lines, a 380 bp (nucleotides 6665-7044)
427 fragment of *FLAM8* (Tb927.2.5760), flanked by 5' HindIII and 3' XhoI restriction sites
428 to facilitate subsequent cloning, was selected using the RNAit2 algorithm
429 (https://dag.compbio.dundee.ac.uk/RNAit/) to ensure that the targeted sequence was
430 distinct from any other genes to avoid any cross-RNAi effects [41]. This *FLAM8* DNA
431 fragment was synthesized by GeneCust Europe (Dudelange, Luxembourg) and
432 inserted into the HindIII-XhoI digested pZJM vector [39].

433 The pZJM-FLAM8 plasmid was linearized with NotI prior to transfection using
434 nucleofector technology (Lonza, Italy) as described previously [42]. The cell line was
435 further engineered for endogenous tagging of *FLAM8* with an mNeonGreen (mNG) at
436 its C-terminal end by using the p3329 plasmid [43], carrying a *FLAM8* gene fragment
437 corresponding to *FLAM8* ORF nucleotides 8892-9391. Prior to nucleofection, NruI
438 linearization of p3329-FLAM8-mNG plasmid was performed.

439 For *in vivo* experiments in mice, *FLAM8*^{RNAi} parasites were finally modified by
440 integrating a plasmid encoding for the chimeric triple reporter which combines the red-
441 shifted firefly luciferase PpyREH9 and the tdTomato red fluorescent protein fused with
442 a TY1 tag [20]. Transformants were selected with the appropriate antibiotic
443 concentrations: phleomycin (1 µg/mL), blasticidin (5 µg/mL), G418 (2 µg/mL), and
444 puromycin (0.1 µg/mL). Clonal populations were obtained by limiting dilution. Cell
445 culture growth was monitored with an automatic Muse cell analyzer (Merck Millipore,
446 Paris).

447 **Generation of *FLAM8* KO mutants**

448 For generating the *FLAM8* knockout and rescue cell lines, all insert templates were
449 synthesized by GeneCust Europe (Dudelange, Luxembourg). For breaking the first

450 allele, the 300 first nucleotides of the *FLAM8* gene flanking sequences were added on
451 each side of a HYG resistance cassette (Fig. S2). For a complete disruption of the
452 *FLAM8* locus, a second selectable marker (PAC) was flanked with the *FLAM8*-flanking
453 sequence at 5' and by 300 nucleotides of the *FLAM8* ORF (nucleotides 501-800) at 3'.
454 For generating an add-back rescue cell line, due to the large size of the *FLAM8* ORF
455 (9,228 nucleotides), the PAC selection marker was replaced by a BLE marker cassette
456 flanked by the 300 first nucleotides of the *FLAM8* 5' untranslated region (UTR) and by
457 the nucleotides 1 to 500 of the *FLAM8* ORF for reinsertion into the endogenous locus
458 of the knockout clone 1. PCR amplifications of the DNA fragments bearing the *FLAM8*
459 flanking sequences and the appropriate resistance markers were used for
460 nucleofection and generation of all cell lines. The primers used are listed below: 5'-
461 CATGACTTTACGTGTTTGGGCAC-3' (FW, located 82 bp upstream the flanking
462 5'UTR sequence); 5'-CTTGCTTGTTTCTGTTTCGCAAC-3' (RV, 130 bp downstream
463 the flanking 3'UTR sequence, used to replace one WT allele by HYG resistance
464 cassette); 5'- GCACACTAAAACTCATTGAAAGCC-3' (RV, 926 bp downstream the
465 ATG codon of *FLAM8*, used for second WT allele replacement by PAC cassette and
466 rescue line generation). All knockout and rescue cell lines were further transfected to
467 express the chimeric triple reporter protein PpyRE9H/TY1/tdTomato for multimodal *in*
468 *vivo* imaging approaches as described elsewhere [20]. Selection-marker recovery was
469 confirmed by screening individual clones in multi-well plates. Transformants were
470 selected with the appropriate antibiotic concentrations: phleomycin (1 µg/mL),
471 blasticidin (5 µg/mL), puromycin (0.1 µg/mL) and hygromycin (2.5 µg/mL). Clonal
472 populations were obtained by limiting dilution and cell culture growth was monitored
473 with an automatic Muse cell analyzer (Merck Millipore, Paris).

474 Knockout and rescue cell lines were validated by whole-genome sequencing (BGI,
475 Hong Kong). Briefly, genomic DNA from parental and mutant cell lines were sequenced
476 by the HiSeq4000 sequence system (Illumina), generating about 10 million 100-bp
477 reads and compared to that of the *T. brucei brucei* AnTat 1.1E Paris reference strain.
478 In addition, some validation of the construct integrations in mutants were performed by
479 PCR analysis according to standard protocols (Fig. S2 and Table 1).

480 **Table 1.** Oligonucleotides used for PCR validation of the Δ*FLAM8* knockout and rescue
481 cell lines.

Primer	Sequence	Target	
1	CATGACTTTACGTGTTTGGGCAC	*FLAM8* WT allele (82 nt upstream 5'UTR)	F
2	GCACACTAAAACTCATTGAAAGCC	*FLAM8* WT allele (926 nt downstream ATG)	R
3	CGTCCGAGGGCAAAGGAATAG	Hygromycin cassette	R
4	GACCGCGCACCTGGTGCATG	Puromycin cassette	R
5	GTGGCCGAGGAGCAGGACTGA	Phleomycin cassette	R

482 Orientation of primers: F, forward; R, reverse.

483 **Motility analyses**

484 *In silico* 2D tracking was performed as previously described [44]. For each BSF strain,
485 10 to 20 movies were recorded for 20 seconds (50 ms of exposure). Trypanosomes at
486 $1x10^6$ parasites/mL were maintained in matrix-dependent HMI-11 medium containing
487 0,5% or 1.1% methylcellulose at 37°C and were observed under the 10x objective of

488 an inverted DMI-4000B microscope (Leica) coupled to an ORCA-03G (Hamamatsu) or
489 a PRIME 95B (Photometrics) camera. Movies were converted with the MPEG
490 Streamclip V.1.9b3 software (Squared 5) and analyzed with the medeaLAB CASA
491 Tracking V.5.9 software (medea AV GmbH). Results were analyzed as mean ± SD of
492 three independent experiments.

493 ***In vitro* bioluminescence quantification and analysis**

494 To perform the parasite density / bioluminescence intensity assay, BSF parasites were
495 counted, centrifuged, and resuspended in fresh HMI-11 medium. Then, 100 µL of this
496 suspension containing 10^6 parasites were transferred into black clear-bottom 96-well
497 plates and serial 2-fold dilutions were performed in triplicate adjusting the final volume
498 to 200 µL with 300 µg/mL of beetle luciferin (Promega, France). Luciferase activity was
499 quantified after 10 min of incubation with an IVIS Spectrum imager (PerkinElmer).
500 Imaging data analysis was performed with the Living Image 4.3.1 software
501 (PerkinElmer) by drawing regions of interest with constant size for well plate
502 quantification. Total photon flux was calculated after removal of intensity values from
503 WT parasites and / or parasite-free medium corresponding to the background noise.
504 Results were analyzed as mean ± SD of three independent experiments (Fig. S1 and
505 S3 A-B).

506 **Mouse infection and ethical statements**

507 Seven-week-old male BALB/c mice were purchased from Janvier Laboratory (sub-
508 strain BALB/cAnNRj) and used as models for experimental infection and monitoring of
509 the bioluminescence signal with the IVIS Spectrum imager (PerkinElmer). This study
510 was conducted in strict accordance with the recommendations from the Guide for the
511 Care and Use of Laboratory Animals of the European Union (European Directive
512 2010/63/UE) and the French Government. The protocol was approved by the “Comité

513 d'éthique en expérimentation animale de l'Institut Pasteur" CETEA 89 (Permit number:
514 2012-0043 and 2016-0017) and undertaken in compliance with the Institut Pasteur
515 Biosafety Committee (protocol CHSCT 12.131). BR is authorized to perform
516 experiments on vertebrate animals (license #A-75-2035) and is responsible for all the
517 experiments conducted personally or under his supervision. For *in vivo* infections,
518 groups of four and three animals (*FLAM8* knockdown and knockout-infected mice,
519 respectively) were injected intraperitoneally (IP) with 10^5 slender BSF parasites,
520 washed in TDB (Trypanosome Dilution Buffer: 5 mM KCl, 80 mM NaCl, 1 mM
521 $MgSO_4$*$7H_2O$, 20 mM Na_2HPO_4, 2 mM NaH_2PO_4, 20 mM glucose) and resuspended
522 in 100 µl of PBS prior animal inoculation. To study the effects of the genotype factor
523 (*FLAM8* knockdown) on parasitemia and EV parasite densities (variables), the most
524 adapted statistical analysis was a multiple comparison of the means of 5 groups by
525 ANOVA, using two-sided tests on the 5 experimental groups. With 3 individuals per
526 group, mixed into 3 cages (5 individuals per cage) to limit any cage effect, the
527 experimental design allows us to obtain significative results for strong effects superior
528 to 1.13 with 0.05% confidence and a power fixed at 0.8. This experiment was
529 performed in two independent replicates.

530 ***In vivo* bioluminescence imaging (BLI) analyses**

531 Infection with bioluminescent parasites was monitored daily by detecting the
532 bioluminescence signal in whole animals with the IVIS Spectrum imager (PerkinElmer).
533 The equipment consists of a cooled charge-coupled camera mounted on a light-tight
534 chamber with a nose cone delivery device to keep the mice anaesthetized during
535 image acquisition with 1.5-2% isoflurane. A heated stage is comprised within the IVIS
536 Spectrum imager to maintain optimum body temperature. D-luciferin potassium salt
537 (Promega) stock solution was prepared in sterile PBS at 33.33 mg/mL and stored in a

538 -20°C freezer. To produce bioluminescence, mice were inoculated by the
539 intraperitoneal route (IP) with 150 µL of D-luciferin stock solution (250 mg/Kg body
540 weight). After 10 minutes of incubation to allow substrate dissemination, all mice were
541 anaesthetized in an oxygen-rich induction chamber with 1.5-2% isoflurane, and dorsal
542 and ventral BLI images were acquired by using automatic exposure (0.5 seconds to 5
543 minutes) depending on signal intensity.
544 Images were analyzed with the Living Image software version 4.3.1 (PerkinElmer).
545 Data were expressed in total photons/second (p/s) corresponding to the total flux of
546 bioluminescent signal according to the selected area (ventral and dorsal regions of
547 interest with constant size covering the total body of the mouse). The background noise
548 was removed by subtracting the bioluminescent signal of the control mouse from the
549 infected ones for each acquisition. For parasite dissemination analyses, a minimum
550 value of photons/second (p/s) was set for all animals in every time point to quantify the
551 exact dissemination area (in cm^2) over the whole animal body. Parasitemia was
552 determined daily following tail bleeds and assayed by automated fluorescent cell
553 counting with a Muse cytometer (Merck-Millipore, detection limit at 10^2 parasites/mL)
554 according to the manufacturer's recommendations. The quantification of the total
555 intravascular parasite population was assessed by calculating the blood volume of all
556 animals according to their body weight and referring to daily parasitemia.
557 To quantify the total number of parasites by BLI (intravascular plus extravascular
558 trypanosomes), an *in vivo* standard curve was performed (Fig. S3 C-D). Since the
559 bioluminescent emission of cultured parental, KO subclones and rescue parasites was
560 not significantly different (Fig. S3 A-B), the *in vivo* standard curve was obtained by
561 injecting IP increasing numbers (10^3, 10^4, 10^5, 10^6 and 10^7 parasites/animal) of
562 parental trypanosomes only (Fig. S3 C-D). After 2.5h, animals received 150 µL of D-

563 luciferin stock solution IP (250 mg/kg body weight), 10 minutes prior image acquisition.
564 During this time, mice were anaesthetized with 1.5-2% isoflurane, and images were
565 acquired in the IVIS Spectrum imager by using automatic exposure settings. A region
566 of interest with a constant size was used to correlate the number of injected parasites
567 with the whole-body BLI signal. Non-infected controls were imaged and the total BLI
568 values used to subtract the background signal or noise. The signals in photons/second
569 were used to construct a standard curve to further interpolate the total number of
570 trypanosomes present in each animal during the entire experimental infection period
571 (Fig. S3 D). Subsequently, to obtain the number of extravascular parasites, the
572 calculated total number of parasites present in the vascular system was subtracted
573 from the total number of trypanosomes per animal body, resulting in estimating the
574 total parasite population colonizing the extravascular compartments at a given time
575 point.

576 **Endothelial transmigration assay**

577 Single donor cryopreserved Primary Human Umbilical Vein Endothelial Cells
578 (HUVECs) were obtained from Promocell and maintained as per the manufacturer's
579 instructions in 75 cm^2 flasks at 37°C with 5% CO_2 in endothelial cell growth medium
580 (Promocell) with 100 U/mL penicillin, and 100 µg/mL streptomycin (Gibco). Cells were
581 passaged at 80-90% confluence by dissociation with 0.04% Trypsin-0.03% EDTA
582 (Promocell), split at 1:3-1:5 ratios, and maintained for up to six passages. Polyester
583 transwell inserts for 24 well plates with 3 µm pore size (Corning) were coated with 10
584 µg/mL bovine fibronectin (Promocell) for one hour, the excess removed, and 600 µL
585 pre-warmed endothelial cell growth medium added to the lower chamber (Fig 6A). The
586 upper chamber was seeded with $2x10^4$ HUVECs per insert in a volume of 100 µL
587 endothelial cell growth medium. Media was exchanged in the upper and lower chamber

588 every two days until monolayer confluence reached (approximately 6 days).
589 Confluence was confirmed by FITC-dextran permeability assay and crystal violet
590 staining of a sacrificed transwell. Briefly, 1 mg/mL FITC-70kDa dextran (Sigma-Aldrich)
591 in endothelial cell growth medium was added to the upper chamber, incubated for 20
592 minutes and leakage to the lower chamber measured on a Qubit 4 Fluorometer
593 (Invitrogen). Leakage of <1% of the FITC-dextran was observed at confluence.
594 Monolayer integrity was confirmed by brightfield imaging of a transwell insert stained
595 with crystal violet as per the manufacturer's instructions (Millipore). To perform the
596 trypanosome transmigration assays, the confluent transwells were exchanged into a
597 new 24 well plate containing pre-warmed assay media (endothelial cell growth medium
598 supplemented with 20% trypanosome growth media) for two hours prior to performing
599 the assay. Cultured trypanosomes were collected by centrifugation at 900×g for 5 min
600 and resuspended in assay media at $2x10^6$/mL. The media in the upper chamber was
601 replaced with 100 µL of assay media containing $2x10^5$ trypanosomes and incubated
602 overnight at 37°C, 5% CO_2. Each cell line was tested in triplicate transwells. Unbiased
603 quantification of trypanosome transmigration was determined after 24 hours by
604 collecting the media from the upper and lower chambers and transferring 100 µL to 96
605 well plates for automated counting using a Guava Easycyte HT system with a green
606 laser and a custom counting protocol for tdTomato fluorescent trypanosomes. The cell
607 counts per ml were used to calculate the number of trypanosomes in each
608 compartment and proportion of transmigration into the lower chamber. Trypanosome
609 transmigration was compared between the FLAM8 mutant cell lines and the parental
610 reference cell line using the Generalised Linear Model function in R with a Gaussian
611 family function and proportion transmigration as the dependant variable. A probability
612 value of $p<0.05$ was considered significant.

613 ***Ex vivo* RT-qPCR of mouse tissues**

614 *Biological samples*. After four weeks of *in vivo* monitoring, parental-, KO- and rescue-
615 infected mice were euthanized by an overdose of an anesthetic/analgesic mixture of
616 ketamine and xylazine (100 mg/kg and 10 mg/kg, respectively). Terminal bleeding was
617 then performed through the inferior *vena cava*, and the collected blood was directly
618 transferred in 1 ml RNAlater (ThermoFisher Scientific), snap frozen in liquid nitrogen
619 for long-term preservation. Next, perfusion was initiated by injecting 0.9% NaCl (pre-
620 heated at 37°C), to completely remove the blood from the animal's body (both organs
621 and vasculature), thus ensuring that subsequent analyses would only contain tissue-
622 dwelling trypanosomes. Finally, spleen, lungs, kidney, gut, testis, liver and skin tissue
623 samples were preserved in 1 ml RNAlater, snap frozen and stored in liquid nitrogen.

624 *RNA isolation*. Total RNA from samples was isolated using the QIAzol Reagent
625 (Qiagen) according to the manufacturer's instructions. Frozen tissue samples were
626 weighed and processed on ice to prevent thawing. Briefly, 30 mg of tissue were added
627 to 700 µl of QIAzol lysis reagent, or 250 µl of blood in 550 µl of QIAzol lysis reagent,
628 and samples were homogenized using the Precellys Evolution Homogenizer (Bertin,
629 USA) with 2.8 mm stainless steel beads for 2 cycles of 1 min at 5000 rpm each,
630 followed by 15 sec of resting between them. Homogenates were then incubated for 5
631 min at room temperature before the addition of 140 µl chloroform (0.2 volume of
632 starting QIAzol lysis reagent), thoroughly mixed by vortexing for 15 seconds, incubated
633 5 min at room temperature and centrifuged at 12,000×g, 4°C, 15 min. The aqueous
634 phase containing the RNA was subsequently mixed with 1.5 volumes of absolute
635 ethanol and transferred into a RNeasy Mini spin column (Qiagen) following the
636 manufacturer's recommendations. The concentration of each RNA sample was
637 measured by spectrophotometric analysis in a NanoDrop 2000c (ThermoFisher

638 Scientific). Finally, RNA quality was determined by capillary electrophoresis in a 2100
639 Bioanalyzer (Agilent). Extracted RNA was stored at -80 °C prior to RT-qPCR analyses.
640 *DNAse treatment and validation*. Extracted RNA samples were subjected to a second
641 DNase treatment using Invitrogen's DNA-*free* kit (Life Technologies) according to
642 manufacturer's protocol. DNase treatment confirmation was performed by running a
643 qPCR targeting the *Tubulin* locus as housekeeping gene control. The primer pair used
644 is as follows: forward (FW), 5'-ACTGGGCAAAGGGCCACTAC-3'; reverse (RV), 5'-
645 CTCCTTGCAGCACACATCGA-3', with an amplicon size of 105 bp. Reactions were
646 done in a volume of 20 µl containing: 1 µl of RNA template (17 ng), 10 µl of 2X GoTaq
647 qPCR Master Mix Buffer, 2 µl of both FW and RV primers (at 10X) and 5 µl of Nuclease-
648 Free Water. Amplification was accomplished in a QuantStudio 3 thermal cycler
649 (Applied Biosystems) using the following program: 2 min at 95°C; 40 cycles at 94°C
650 15 sec; 55°C 1 min; and final 30 sec at 60°C. The absence of residual DNA in the
651 DNAse-treated RNA samples was thus confirmed when no amplification was
652 observed. RNA samples were further employed for gene expression quantification.
653 *Primer design of target genes*. For *FLAM8* amplification, primers were designed to
654 recognize the 324-bp region suppressed during *FLAM8* knockout generation: FW, 5'-
655 GCATCGTTCGTGAGGTTGGA-3'; RV, 5'-GTTCCTCTTCGTCATCTGGTTCA-3'. The
656 amplicon size was 88 bp. For Protein Associated to Differentiation 1 (PAD1)
657 quantification in infected samples, primer sequences were described elsewhere
658 (Saldivia et al. 2016) and are listed below: FW, 5'-
659 TCATGGTTTCGCCATTCTCGTAACC-3'; RV, 5'-
660 CTCAGCCACTTCTCTCCTACAACAC-3'. Amplicon size is 156 bp.
661 *Real time RT-PCR assay*. One step RT-PCR kit (Promega) was used. Reactions were
662 prepared in a volume of 20 µl, containing: 1 µl of RNA template (17 ng), 10 µl of 2X

663 GoTaq qPCR Master Mix Buffer, 0.4 µl of 50X GoScript RT Mix for 1-Step RT-qPCR,
664 2 µl of both FW and RV primers (10X), and 4,6 µl of Nuclease-Free Water. Reverse
665 transcription and amplification were accomplished in one step in a QuantStudio 3
666 thermal cycler (Applied Biosystems) using the following incubation program: 15 min at
667 42°C; 10 min at 95°C; 40 cycles of 95°C during 30 sec; 55°C for *Tubulin*, 58°C for
668 *FLAM8* or 60°C for *PAD1* during 1 min; final 72°C during 30 sec. A melt curve program
669 was included: 15 sec at 95°C; 55°C for *Tubulin*, 58°C for *FLAM8* or 60°C for *PAD1*
670 during 1 min; 95°C for 10 sec. Amplicons were then analyzed by gel electrophoresis.
671 Negative and positive controls consisted of RNA extracted from uninfected mice and
672 cultured trypanosomes, respectively.

673 **Table 2.** Oligonucleotides used for *ex vivo* RT-qPCR of infected tissues.

Primer		Sequence	Purpose
Tubulin	F	ACTGGGCAAAGGGCCACTAC	Housekeeping control. Total trypanosome quantification (both SL and ST parasites) through standard curve generation.
	R	CTCCTTGCAGCACACATCGA	
FLAM8	F	GCATCGTTCGTGAGGTTGGA	Detection of parasites expressing *FLAM8*. The amplified sequence is absent in *FLAM8* KO mutants.
	R	GTTCCTCTTCGTCATCTGGTTCA	
PAD-1	F	TCATGGTTTCGCCATTCTCGTAACC	Quantification of transmissible ST parasites within *ex vivo* samples.
	R	CTCAGCCACTTCTCTCCTACAACAC	

674 Orientation of primers: F, forward; R, reverse.

675 *RT-qPCR data analysis*. All samples were amplified in triplicates and Cq mean values
676 were calculated. Considering that the same initial amounts of total mRNAs extracted
677 from each organ were used as RT-qPCR templates, the total number of parasites in
678 each sample was calculated for comparisons by using a *Tubulin* RT-qPCR standard
679 curve. Nine pools of cultured parasites (p) increasing by 10-folds from 10^1 to 10^8 were
680 extracted and tested in triplicates by *Tubulin* RT-qPCR to generate a standard curve.
681 The resulting standard curve's equation Cq = -2,87 x Log10(p) + 35,412 allowed us to
682 calculate the total number of parasites per mg of sample according to the Cq values
683 obtained by *Tubulin* RT-qPCR on each sample. For normalization purposes to better
684 compare the variations of the parasite populations in each compartment between
685 strains, the difference between the number of parasites in each tissue sample of a
686 given mouse and the number of parasites in the blood sample from the same mouse
687 was calculated and plotted as Delta number of parasites. *Tubulin* expression (CqTub)
688 was also used to normalize the *PAD1* mRNA levels (CqPAD1): the difference between
689 the CqPAD1 and the CqTub values was calculated for each organ of each mouse and
690 plotted as the Delta CqPAD1-CqTub. It allowed us to compare the relative proportions
691 of parasites expressing *PAD1* mRNAs between organs and strains, a higher Delta
692 CqPAD1-CqTub correlating with a lower amount of *PAD1* transcripts in the organ.

693 **Immunofluorescence analysis (IFA)**

694 Cultured parasites were washed twice in TDB and spread directly onto poly-L-lysine
695 coated slides. For methanol fixation, slides were air-dried for 10 min, fixed in methanol
696 at -20°C for 30 seconds and rehydrated for 20 min in PBS. For immunodetection, slides
697 were incubated for 1 h at 37°C with the appropriate dilution of the first antibody in 0.1%
698 BSA in PBS. After 3 consecutive 5 min washes in PBS, species and subclass-specific
699 secondary antibodies coupled to the appropriate fluorochrome (Alexa 488, Cy3, Cy5

700 Jackson ImmunoResearch) were diluted 1/400 in PBS containing 0.1% BSA and were
701 applied for 1 h at 37°C. After washing in PBS as indicated above, slides were finally
702 stained with 4',6-diamidino-2-phenylindole (DAPI, 1 µg/mL) for visualization of
703 kinetoplast and nuclear DNA content and mounted under cover slips with ProLong
704 antifade reagent (Invitrogen), as previously described [8]. Slides were observed under
705 an epifluorescence DMI4000 microscope (Leica) with a 100x objective (NA 1.4), an
706 EL6000 (Leica) as light excitation source and controlled by the Micro-Manager V1.4.22
707 software (NIH), and images were acquired using an ORCA-03G (Hamamatsu) or a
708 PRIME 95B (Photometrics) camera. Images were analyzed with ImageJ V1.8.0 (NIH).
709 The monoclonal antibody mAb25 (anti-mouse IgG2a, 1:10) was used as a flagellum
710 marker as it specifically recognizes the axoneme protein *Tb*SAXO1 [45]. FLAM8 was
711 detected using: i) a specific rabbit serum (1:500) kindly provided by Paul McKean
712 (University of Lancaster, UK), or ii) a monoclonal anti-mNeonGreen antibody (anti-
713 mouse IgG2c, 1:100, ChromoTek). CARP3 was detected using a polyclonal CARP3
714 antiserum (1:150) [21]. Stumpy BSF were identified at the molecular level with a rabbit
715 polyclonal anti-PAD1 antibody (kindly provided by Keith Matthews, University of
716 Edinburgh; dilution 1:300) [46]. In the case of RNAi knockdown experiments, IFA
717 signals were normalized using the signal obtained in non-induced controls as a
718 reference.

719 **Measurements, normalization, and statistical analyses**

720 Standardization of fluorescent signals was carried out by parallel setting of raw
721 integrated density signals in all the images to be compared in ImageJ V1.8.0 (NIH).
722 For clarity purposes, the brightness and contrast of several pictures were adjusted
723 after their analysis in accordance with editorial policies. Statistical analyses and plots
724 were performed with XLSTAT 2019.2.01 (Addinsoft) in Excel 2016 (Microsoft) or Prism

725 V9.3.1 (GraphPad). Statistical analyses include: (1) linear regression for
726 bioluminescence / fluorescence intensity vs. parasite density and RT-qPCR standard
727 curve, (2) two-sided ANOVA tests with Tukey or Dunnett's ad-hoc post-tests for inter-
728 group comparisons for growth curves, IV / EV parasite populations and parasite
729 dissemination, and ΔCq comparisons of RT-qPCR data, all at 95% confidence.

730 **Acknowledgements**

731 We thank M. Bonhivers, D. Robinson, P. McKean, K. Matthews, and K. Gull for
732 providing various plasmids and antibodies. We gratefully acknowledge the UTechS
733 Photonic BioImaging (Imagopole), C2RT, Institut Pasteur, supported by the French
734 National Research Agency (France BioImaging; ANR-10–INSB–04; Investments for
735 the Future). We are grateful to P. Bastin for his strong scientific and human support.
736 We warmly thank M. Boshart, P. Bastin, and S. Bonnefoy for their critical reading of
737 the manuscript.

738 **Funding**

739 None of these funding sources has a direct scientific or editorial role in the present
740 study. This work was supported by the Institut Pasteur. This work was supported by
741 the French Government Investissement d'Avenir programme, Laboratoires
742 d'Excellence ANR-10-LABX-62-IBEID and ANR-11-LABX-0024-ParaFrap, and the
743 French National Agency for Scientific Research via the projects ANR-14-CE14-0019-
744 01 EnTrypa, ANR-18-CE15-0012 TrypaDerm, and ANR-19-CE15-0004-02 AdipoTryp.
745 EC, JMTN, CT and PS were/are funded on these ANR grants. BR and AlC are funded
746 by the Institut Pasteur and AiC by the Institut Pasteur of Guinea. AML and AnC are
747 funded by a Wellcome Senior Fellowship to AML (209511/Z/17/Z). The funders had no
748 role in study design, data collection and analysis, decision to publish, or preparation of
749 the manuscript.

750 **Author contributions**

751 ECA and BR designed the study. ECA, JMTN, PS, CT, AnC and AlC performed the
752 experiments. ECA, JMTN, AnC, AiC and BR analyzed the data. ECA and BR wrote the

753 manuscript. ECA, AnC, AMC and BR discussed the manuscript. BR acquired the
754 funding.

755 **Competing interest**

756 All authors declare no financial relationships with any organizations that might have an
757 interest in the submitted work in the previous three years, no other relationships or
758 activities that could appear to have influenced the submitted work, and no other
759 relationships or activities that could appear to have influenced the submitted work.

760 **Figure captions**

761

762 **Figure 1. Characterization of the *FLAM8::mNG FLAM8^{RNAi}* strain *in vitro* and *in***
763 ***vivo* functional investigation in the mammalian host. A)** Expression of *FLAM8*
764 mRNA assessed by RT-PCR by the comparative $\Delta\Delta C_T$ method in control, non-induced
765 and induced *FLAM8::mNG FLAM8^{RNAi}* parasites (72 h). **B)** Immunofluorescence
766 pictures of non-induced (upper panels) and induced (bottom panels) *FLAM8::mNG*
767 *FLAM8^{RNAi}* BSF during 72 h. Methanol-fixed trypanosomes were stained with an anti-
768 mNG antibody (green) and DAPI for DNA content (blue). The scale bars represent 5
769 µm. **C)** Growth curves of control, non-induced and induced *FLAM8::mNG FLAM8^{RNAi}*
770 BSF parasites. All cell lines received 1 µg tetracycline for 6 days. Control parasites are
771 Lister 427 "Single Marker" BSF parasites that do not bear the pZJM-FLAM8 plasmid
772 for RNAi silencing. Results represent the mean (± standard deviation, SD) of three
773 independent experiments. **D)** Groups of 4 BALB/c mice were injected IP with either
774 control, non-induced or induced *FLAM8^{RNAi}* BSF trypanosomes. One PBS-injected
775 BALB/c animal was used as negative control. Representative normalized *in vivo*
776 images of the bioluminescence radiance signal (in photons / second / cm^2 / steradian)
777 emitted from BALB/c mice infected with control, non-induced and induced
778 *FLAM8::mNG FLAM8^{RNAi}* parasites 4 days post-infection (non-infected technical
779 control mice were negative for bioluminescence, not shown). RNAi silencing of *FLAM8*
780 was maintained *in vivo* by the addition of doxycycline in sugared drinking water 48 h
781 prior infection and until the end of the experiment. **E)** Number of parasites in the blood
782 (intravascular, IV) of infected BALB/c mice during the course of the infection (5 days)
783 counted from a tail bleed using a cytometer. **F)** Number of parasites in the
784 extravascular compartment (extravascular, EV) of the same infected mice as in E). **G)**

785 Dissemination of control, non-induced and induced *FLAM8::mNG FLAM8*^{RNAi}
786 parasites, measured over the entire animal body (in cm^2) through the total
787 bioluminescent surface, during the entire infection course. Results represent means ±
788 standard deviation (SD).
789
790 **Figure 2. Characterization of Δ*FLAM8* null mutants *in vitro*. A)**
791 Immunofluorescence pictures of parental, Δ*FLAM8* knockout and rescue pleomorphic
792 BSF parasites labelled with the anti-FLAM8 (green) and mAb25 (axoneme in magenta)
793 antibodies, DAPI staining for DNA content (blue). Scale bars show 5 µm. **B)**
794 Quantification of the total fluorescence intensity of FLAM8 along the entire flagellum
795 length in methanol-fixed parental, Δ*FLAM8* knockout and rescue parasites. **C)** Growth
796 curve of one parental, three Δ*FLAM8* subclones and one rescue pleomorphic BSF
797 trypanosome cell lines over 6 consecutive days. **D)** Measurements of the flagellum
798 length based on the axonemal marker mAb25 profiles in parental, three Δ*FLAM8*
799 subclones and rescue parasites. No statistical differences were found. **E-H)** Motility
800 tracking analysis showing the average speeds (E and G) and linearity (F and H) of BSF
801 cell lines in matrix-dependent culture medium containing 0.5% (E-F) or 1.1% (G-H)
802 methylcellulose. No statistical differences were observed. The number of parasites
803 considered for quantifications (N) is indicated under and above graphs in (B) and (D-
804 H), respectively. Results represent the mean ± standard deviation (SD) of three
805 independent experiments. Statistical tests included one-way ANOVA and Tukey's ad-
806 hoc post-tests for multiple comparisons.
807
808 **Figure 3. Functional investigations on the Δ*FLAM8* null mutants *in vivo* in the**
809 **mammalian host.** Groups of 3 BALB/c mice were injected IP with either one parental,

810 three ΔF*LAM8* null subclones or one rescue strains. One PBS-injected BALB/c animal
811 was used as negative control. **A)** Normalized *in vivo* images of the bioluminescence
812 radiance intensity (in photons / second / cm^2 / steradian) emitted 8 days post-infection
813 in BALB/c mice infected with parental, three Δ*FLAM8* subclones or rescue parasites
814 (non-infected control mice C- were negative for bioluminescence). **B)** Total number of
815 parasites in the blood of infected mice (intravascular, IV) daily counted from tail bleeds
816 using a cytometer over 4 weeks. Statistically significant differences ($p<0.01$) are
817 indicated with one, two or three asterisks (*, **, ***) representing differences between
818 the parental strain and one, two or three Δ*FLAM8* subclones, respectively. **C)** Total
819 number of extravascular (EV) trypanosomes in the same mice. Statistically significant
820 differences between the parental strain and Δ*FLAM8* subclones are indicated as in B).
821 **D-E)** Variations of the total numbers of intravascular (IV as in B) and extravascular (EV
822 as in C) parasite populations in the same mice plotted as fold differences to values
823 obtained with mice infected with parental trypanosomes at the same time point. **F)**
824 Dissemination of the parental, three Δ*FLAM8* subclones and rescue parasite strains,
825 measured over the entire animal body (in cm^2) through the total surface of
826 bioluminescent signal, during the entire infection course. Statistically significant
827 differences between the parental strain and Δ*FLAM8* subclones are indicated as
828 described above. Results represent means ± standard deviation (SD). Statistical tests
829 included two-way ANOVA and Tukey's ad-hoc post-tests for multiple comparisons in
830 B-F. Detailed individual data are provided in Fig. S4.
831
832 **Figure 4. The absence of *FLAM8* reduces extravascular trypanosome**
833 **dissemination.** In a second experimental infection, groups of 3 BALB/c animals were
834 injected IP with either parental, three ΔF*LAM8* null subclones or rescue strains, while

835 one PBS-injected BALB/c animal was used as negative control. At day 24 post-
836 infection, animals were euthanized, and the gut, kidney, liver, lung, skin, spleen and
837 testes were collected to quantify the parasite proportion in each organ. **A)** Total number
838 of intravascular parasites (IV) during the infection period. **B)** Total number of
839 extravascular (EV) trypanosomes in the same mice. **C)** Dissemination of the parental,
840 three Δ*FLAM8* subclones and rescue parasite strains, measured over the entire animal
841 body (in cm^2) through the total surface of bioluminescent signal, during the entire
842 infection course. Statistically significant differences ($p<0.01$) are indicated with one or
843 three asterisks (*, ***) representing differences between the parental strain and one or
844 three Δ*FLAM8* subclones, respectively. Detailed individual data are provided in Fig.
845 S5. **D)** Delta number of parasites per dissected organs and strains. The total number
846 of parasites in each sample was calculated per mg of tissues by using a *Tubulin* RT-
847 qPCR standard curve. To better compare the variations of the parasite populations in
848 each compartment between strains, the Delta number of parasites was calculated as
849 the difference between the number of parasites in each tissue sample of a given mouse
850 and the number of parasites in the blood sample from the same mouse. **E)** Delta
851 number of parasites per strain calculated as the average of values for individual organs
852 shown in D. Statistical differences ($p<0.0001$) according to one-way ANOVA and
853 Dunnett's comparison tests. Detailed individual data are provided in Table S1 and Fig.
854 S6.
855
856 **Figure 5. Parasite differentiation is not impacted in *FLAM8*-depleted**
857 **trypanosomes. A)** Representative immunofluorescence pictures of stumpy parasites
858 after *in vitro* differentiation from proliferative slenders of parental (left panel), three
859 Δ*FLAM8* subclones (middle panels) and rescue (right panel) parasite strains upon *in*

860 *vitro* treatment with a nucleotide 5'-AMP analog. Methanol-fixed parasites were
861 labelled with the anti-PAD-1 antibody (red), and DAPI staining for DNA content (blue).
862 Scale bars show 5 µm. **B)** Quantification of the proportion of stumpy trypanosomes in
863 all pleomorphic cell lines after *in vitro* differentiation. The number of parasites
864 considered for quantification (n) is indicated above the graph. No significant differences
865 were found (one-way ANOVA and Tukey's comparisons test). Results represent the
866 mean ± standard deviation (SD) of three independent experiments. **C)** Selected
867 immunofluorescence images of freshly *in vitro* differentiated procyclic cells.
868 Trypanosomes were doubly labelled with anti-FLAM8 (green) and mAb25 (axoneme
869 in magenta), DAPI staining showing DNA content in blue. Scale bars show 5 µm. **D)**
870 Upon differentiation, procyclic forms (PCF) of parental, three Δ*FLAM8* subclones and
871 rescue parasite strains were equally diluted, and their *in vitro* growth assessed.
872 Statistical differences ($p<0.01$) were observed only when comparing parental and KO
873 2 PCF trypanosomes (one-way ANOVA and Tukey's comparison test). Results
874 represent the mean ± standard deviation (SD) of four independent experiments. **E)**
875 Average relative proportions of *PAD-1* expression levels quantified by RT-qPCR on
876 blood and dissected organs at day 24 of the second *in vivo* challenge. *Tubulin*
877 expression was used to normalize the *PAD-1* mRNA levels in all parental-, Δ*FLAM8*-
878 and rescue-infected mice samples. **F)** Representative immunofluorescence images of
879 naturally differentiated stumpy trypanosomes from parental, one selected Δ*FLAM8*
880 subclone and rescue strains isolated from mouse blood during the first peak of
881 parasitemia (first experimental *in vivo* infection). Parasites were labelled with anti-PAD-
882 1 antibody (red), and DAPI staining for DNA content (blue). Scale bars show 5 µm.
883

884 **Figure 6. Parasites lacking *FLAM8* are impaired in transmigrating through**
885 **endothelial cells *in vitro*. A)** Schematic representation of the trans-endothelial
886 migration assay, showing the transwell system (Boyden chamber) containing the upper
887 and the lower compartments, the monolayer of endothelial HUVEC cells and slender
888 trypanosomes seeded on the top of the chamber for 24 hours. **B)** After this period,
889 parasites within the upper and lower chambers were counted and values further used
890 to calculate the proportion of parental, three Δ*FLAM8* subclones and rescue parasites
891 that migrated through the endothelial monolayer into the lower compartment.
892 Trypanosome transmigration was compared between the FLAM8 mutant cell lines and
893 the parental reference line (100% of trans-endothelial migration) using the Generalised
894 Linear Model function in R with a Gaussian family function and proportion of
895 transmigration as the dependent variable. A probability value of $p<0.001$ was
896 considered significant (*). Error bars show SD. **C)** Representative immunofluorescence
897 images of cultured slender trypanosomes from parental, Δ*FLAM8* subclone and rescue
898 strains. Methanol-fixed parasites were labelled with anti-CARP3 antibody (green
899 intensity normalized), and DAPI staining for DNA content (blue). Scale bars show 5
900 µm. **D)** Quantification of CARP3 fluorescence signal in normalized images from
901 methanol-fixed parental, Δ*FLAM8* subclones and rescue trypanosomes, expressed as
902 the ratio between the fluorescent CARP3 signal intensity along the entire flagellum
903 divided by the length of individual flagella. The number of parasites considered for
904 quantification (n) is indicated under the graph. Statistical differences ($p<0.0001$)
905 according to one-way ANOVA and Dunnett's comparison test. Results represent the
906 mean ± standard deviation (SD) of two independent experiments.

907 **Supporting information captions**

908

909 **Figure S1. Validation of the triple-reporter efficiency in monomorphic *FLAM8^{RNAi}***
910 **parasite lines.** Linear correlation between the number of parasites and the
911 bioluminescence (in p/s) emitted by monomorphic 427 *FLAM8::mNG FLAM8^{RNAi}* BSF
912 overexpressing the triple reporter chimeric protein [20], acquired by the IVIS Spectrum
913 imager. Parasites without the RNAi plasmid (control, C), non-treated with tetracycline
914 (non-induced, NI) and treated with tetracycline (induced, I) are shown. Representative
915 bioluminescent image of serial 1/2 dilutions performed in a 96-well plate (in photons /
916 second / cm^2 / steradian). RNAi induction was triggered by the addition of 1 µg
917 tetracycline and / or doxycycline for 72 h. Results represent the mean ± standard
918 deviation (SD) of three independent experiments.

919

920 **Figure S2. Molecular validation of the Δ*FLAM8* null mutant cell lines. A)** Whole-
921 genome sequencing results showing *FLAM8* wild-type allele (WT, upper panel), the
922 partial loss of the 5' *FLAM8* ORF in Δ*FLAM8* knockout trypanosomes (middle panel;
923 the black arrow is showing the absence of reads at the *FLAM8* 5' ORF in the knockout
924 line); and the restoration of the full *FLAM8* gene in rescue parasites (bottom panel; the
925 black arrow is showing the absence of reads within the *pac* cassette due to the
926 insertion of the new construct bearing the *ble* resistance marker), relative to the
927 number of reads per 100-nt read length. The presence of the correct antibiotic
928 cassettes is shown for knockout and rescue parasites (right middle and bottom panels).
929 Δ*FLAM8* knockout and rescue parasites also bear a construct for expression of a triple
930 reporter (TR) as assessed by the detection of *bsd* reads. **B)** Schemes showing the
931 structure of the *FLAM8* locus in wild-type parasites (upper scheme) and the integration

932 plan of the different cassettes for Δ*FLAM8* knockout (middle panel, *HYG*- and *PAC*-
933 containing schemes) and Rescue parasites (lower panel *HYG*- and *BLE*-containing
934 schemes). **C)** PCR confirmation of the successful integrations of all reporter cassettes.
935 Primer pairs used for PCRs are indicated at the bottom of each line and correspond to
936 those drawn on the schemes in B), along with the expected band sizes of the
937 corresponding diagnostic PCR. BSD: blasticidin; HYG: hygromycin; PAC: puromycin;
938 BLE: phleomycin.
939
940 **Figure S3. *In vitro* and *in vivo* validation of the triple-reporter efficiency in**
941 **pleomorphic Δ*FLAM8* mutant cell lines. A)** Representative bioluminescent image
942 (in photons / second) of serial 1/2 dilutions performed in a 96-well plate of pleomorphic
943 parental, Δ*FLAM8* knockout subclones and rescue parasites overexpressing the triple
944 reporter chimeric protein [20]. **B)** Linear correlation between the number of parasites
945 and the emitted bioluminescence (in photons / second) acquired by the IVIS Spectrum
946 imager. Results represent the mean ± standard deviation (SD) of three independent
947 experiments. **C)** Representative ventral view images of mice infected with increasing
948 amounts of parental trypanosomes (10^3, 10^4, 10^5, 10^6 and 10^7 parasites/animal)
949 acquired with the IVIS Spectrum imager 2.5 hours after IP injection. **D)** *In vivo* standard
950 curve showing the correlation between the number of injected parasites and the
951 bioluminescent signal (in photons/second, R^2 = 1). The standard curve was further
952 employed to calculate the total number of parasites present in infected animals through
953 whole-body BLI signal.
954
955 **Figure S4: The absence of *FLAM8* reduces extravascular trypanosome**
956 **dissemination.** Detailed individual data used in Fig. 3. Groups of BALB/c mice were

957 injected IP with either one parental, three ΔF*LAM8* null subclones or one rescue
958 strains. Total number of parasites in the blood of infected mice (intravascular, IV) daily
959 counted from tail bleeds using a cytometer over 4 weeks (left graphics). Total number
960 of extravascular trypanosomes quantified from bioluminescence images in the same
961 mice (middle graphs). Dissemination measured over the entire animal body (in cm^2)
962 through the total surface of bioluminescent signal (right graphs).
963
964 **Figure S5. Functional investigations on the Δ*FLAM8* null mutants *in vivo* in the**
965 **mammalian host.** Detailed individual data used in Fig. 4. Groups of BALB/c mice were
966 injected IP with either one parental, three ΔF*LAM8* null subclones or one rescue
967 strains. Total number of parasites in the blood of infected mice (intravascular, IV)
968 counted from tail bleeds using a cytometer over 3.5 weeks (left graphs). Total number
969 of extravascular trypanosomes quantified from bioluminescence images in the same
970 mice (middle graphs). Dissemination measured over the entire animal body (in cm^2)
971 through the total surface of bioluminescent signal (right graphics).
972
973 **Figure S6.** Detailed individual data used in Fig. 4D. Delta number of parasites per
974 dissected organs and strains in each individual mouse. The total number of parasites
975 in each sample was calculated per mg of tissues by using a *Tubulin* RT-qPCR standard
976 curve. **A)** For normalization purposes, the difference between the number of parasites
977 in each tissue sample of a given mouse and the number of parasites in the blood
978 sample from the same mouse was calculated and plotted as Delta number of parasites.
979 **B)** As an alternative normalization method, the ratio between the number of parasites
980 in each tissue sample of a given mouse and the number of parasites in the blood
981 sample from the same mouse was calculated and plotted as EV / IV parasites ratio.

982

983 **Table S1** Detailed qPCR results from the second experimental infection used in Fig.

984 4D-E, Fig. 5E and Fig. S6.

985

986 **References**

987 1. MacGregor P, Szoor B, Savill NJ, Matthews KR. Trypanosomal immune
988 evasion, chronicity and transmission: an elegant balancing act. Nat Rev Microbiol.
989 2012;10(6):431-8. Epub 2012/05/01. doi: 10.1038/nrmicro2779. PubMed PMID:
990 22543519.

991 2. Smith TK, Bringaud F, Nolan DP, Figueiredo LM. Metabolic reprogramming
992 during the *Trypanosoma brucei* life cycle. F1000Res. 2017;6. Epub 2017/06/20. doi:
993 10.12688/f1000research.10342.2. PubMed PMID: 28620452; PubMed Central
994 PMCID: PMCPMC5461901.

995 3. Rotureau B, Van Den Abbeele J. Through the dark continent: African
996 trypanosome development in the tsetse fly. Frontiers in cellular and infection
997 microbiology. 2013;3:53. Epub 2013/09/26. doi: 10.3389/fcimb.2013.00053. PubMed
998 PMID: 24066283; PubMed Central PMCID: PMC3776139.

999 4. Capewell P, Cren-Travaille C, Marchesi F, Johnston P, Clucas C, Benson RA,
1000 et al. The skin is a significant but overlooked anatomical reservoir for vector-borne
1001 African trypanosomes. eLife. 2016;5. doi: 10.7554/eLife.17716. PubMed PMID:
1002 27653219; PubMed Central PMCID: PMCPMC5065312.

1003 5. Caljon G, Van Reet N, De Trez C, Vermeersch M, Perez-Morga D, Van Den
1004 Abbeele J. The Dermis as a Delivery Site of *Trypanosoma brucei* for Tsetse Flies.
1005 PLoS Pathog. 2016;12(7):e1005744. doi: 10.1371/journal.ppat.1005744. PubMed
1006 PMID: 27441553; PubMed Central PMCID: PMCPMC4956260.

1007 6. Trindade S, Rijo-Ferreira F, Carvalho T, Pinto-Neves D, Guegan F, Aresta-
1008 Branco F, et al. *Trypanosoma brucei* Parasites Occupy and Functionally Adapt to the
1009 Adipose Tissue in Mice. Cell Host Microbe. 2016. doi: 10.1016/j.chom.2016.05.002.
1010 PubMed PMID: 27237364.

1011 7. Crilly NP, Mugnier MR. Thinking outside the blood: Perspectives on tissue-
1012 resident *Trypanosoma brucei*. PLoS Pathog. 2021;17(9):e1009866. Epub 2021/09/17.
1013 doi: 10.1371/journal.ppat.1009866. PubMed PMID: 34529724; PubMed Central
1014 PMCID: PMCPMC8445408.
1015 8. Rotureau B, Subota I, Bastin P. Molecular bases of cytoskeleton plasticity during
1016 the *Trypanosoma brucei* parasite cycle. Cell Microbiol. 2011;13(5):705-16. Epub
1017 2010/12/17. doi: 10.1111/j.1462-5822.2010.01566.x. PubMed PMID: 21159115.
1018 9. Broadhead R, Dawe HR, Farr H, Griffiths S, Hart SR, Portman N, et al. Flagellar
1019 motility is required for the viability of the bloodstream trypanosome. Nature.
1020 2006;440(7081):224-7. Epub 2006/03/10. doi: nature04541 [pii]
1021 10.1038/nature04541. PubMed PMID: 16525475.
1022 10. Kohl L, Robinson D, Bastin P. Novel roles for the flagellum in cell
1023 morphogenesis and cytokinesis of trypanosomes. EMBO J. 2003;22(20):5336-46.
1024 Epub 2003/10/09. doi: 10.1093/emboj/cdg518. PubMed PMID: 14532107.
1025 11. Tetley L, Vickerman K. Differentiation in *Trypanosoma brucei*: host-parasite cell
1026 junctions and their persistence during acquisition of the variable antigen coat. J Cell
1027 Sci. 1985;74:1-19. Epub 1985/03/01. PubMed PMID: 4030903.
1028 12. Langousis G, Hill KL. Motility and more: the flagellum of *Trypanosoma brucei*.
1029 Nat Rev Microbiol. 2014;12(7):505-18. Epub 2014/06/17. doi: 10.1038/nrmicro3274.
1030 PubMed PMID: 24931043.
1031 13. Rotureau B, Morales MA, Bastin P, Spath GF. The flagellum-MAP kinase
1032 connection in Trypanosomatids: a key sensory role in parasite signaling and
1033 development? Cell Microbiol. 2009;11(5):710-18. Epub 2009/02/12. doi: CMI1295 [pii]
1034 10.1111/j.1462-5822.2009.01295.x. PubMed PMID: 19207727.

1035 14. Roditi I, Schumann G, Naguleswaran A. Environmental sensing by African
1036 trypanosomes. Curr Opin Microbiol. 2016;32:26-30. Epub 2016/05/01. doi:
1037 10.1016/j.mib.2016.04.011. PubMed PMID: 27131101.
1038 15. Shimogawa MM, Ray SS, Kisalu N, Zhang Y, Geng Q, Ozcan A, et al. Parasite
1039 motility is critical for virulence of African trypanosomes. Sci Rep. 2018;8(1):9122. Epub
1040 2018/06/16. doi: 10.1038/s41598-018-27228-0. PubMed PMID: 29904094; PubMed
1041 Central PMCID: PMCPMC6002391.
1042 16. Subota I, Julkowska D, Vincensini L, Reeg N, Buisson J, Blisnick T, et al.
1043 Proteomic analysis of intact flagella of procyclic *Trypanosoma brucei* cells identifies
1044 novel flagellar proteins with unique sub-localisation and dynamics. Molecular & cellular
1045 proteomics : MCP. 2014. Epub 2014/04/18. doi: 10.1074/mcp.M113.033357. PubMed
1046 PMID: 24741115.
1047 17. Fort C, Bonnefoy S, Kohl L, Bastin P. Intraflagellar transport is required for the
1048 maintenance of the trypanosome flagellum composition but not its length. J Cell Sci.
1049 2016;129(15):3026-41. Epub 2016/06/28. doi: 10.1242/jcs.188227. PubMed PMID:
1050 27343245.
1051 18. Bertiaux E, Morga B, Blisnick T, Rotureau B, Bastin P. A Grow-and-Lock Model
1052 for the Control of Flagellum Length in Trypanosomes. Curr Biol. 2018. Epub
1053 2018/11/20. doi: 10.1016/j.cub.2018.10.031. PubMed PMID: 30449671.
1054 19. Calvo-Alvarez E, Bonnefoy S, Salles A, Benson FE, McKean PG, Bastin P, et
1055 al. Redistribution of FLAgellar Member 8 during the trypanosome life cycle:
1056 Consequences for cell fate prediction. Cell Microbiol. 2021;23(9):e13347. Epub
1057 2021/04/26. doi: 10.1111/cmi.13347. PubMed PMID: 33896083; PubMed Central
1058 PMCID: PMCPMC8459223.

1059 20. Calvo-Alvarez E, Cren-Travaille C, Crouzols A, Rotureau B. A new chimeric
1060 triple reporter fusion protein as a tool for *in vitro* and *in vivo* multimodal imaging to
1061 monitor the development of African trypanosomes and *Leishmania* parasites. Infect
1062 Genet Evol. 2018. Epub 2018/01/18. doi: 10.1016/j.meegid.2018.01.011. PubMed
1063 PMID: 29339220.
1064 21. Bachmaier S, Giacomelli G, Calvo-Alvarez E, Vieira LR, Van Den Abbeele J,
1065 Aristodemou A, et al. A multi-adenylate cyclase regulator at the flagellar tip controls
1066 African trypanosome transmission. Nat Commun. 2022;13(1):5445. Epub 2022/09/17.
1067 doi: 10.1038/s41467-022-33108-z. PubMed PMID: 36114198; PubMed Central
1068 PMCID: PMCPMC9481589.
1069 22. Rojas F, Silvester E, Young J, Milne R, Tettey M, Houston DR, et al.
1070 Oligopeptide Signaling through TbGPR89 Drives Trypanosome Quorum Sensing. Cell.
1071 2018. Epub 2018/12/07. doi: 10.1016/j.cell.2018.10.041. PubMed PMID: 30503212.
1072 23. Goodwin LG. The pathology of African trypanosomiasis. Trans R Soc Trop Med
1073 Hyg. 1970;64(6):797-817. Epub 1970/01/01. PubMed PMID: 5495630.
1074 24. Biteau N, Asencio C, Izotte J, Rousseau B, Fevre M, Pillay D, et al.
1075 *Trypanosoma brucei gambiense* Infections in Mice Lead to Tropism to the
1076 Reproductive Organs, and Horizontal and Vertical Transmission. PLoS Negl Trop Dis.
1077 2016;10(1):e0004350. Epub 2016/01/07. doi: 10.1371/journal.pntd.0004350. PubMed
1078 PMID: 26735855; PubMed Central PMCID: PMCPMC4703293.
1079 25. Carvalho T, Trindade S, Pimenta S, Santos AB, Rijo-Ferreira F, Figueiredo LM.
1080 *Trypanosoma brucei* triggers a marked immune response in male reproductive organs.
1081 PLoS Negl Trop Dis. 2018;12(8):e0006690. Epub 2018/08/16. doi:
1082 10.1371/journal.pntd.0006690. PubMed PMID: 30110342; PubMed Central PMCID:
1083 PMCPMC6093638.

1084 26. Caljon G, Van Den Abbeele J, Sternberg JM, Coosemans M, De Baetselier P,
1085 Magez S. Tsetse fly saliva biases the immune response to Th2 and induces anti-vector
1086 antibodies that are a useful tool for exposure assessment. Int J Parasitol.
1087 2006;36(9):1025-35. Epub 2006/06/17. doi: 10.1016/j.ijpara.2006.05.002. PubMed
1088 PMID: 16777113.
1089 27. Camara M, Soumah AM, Ilboudo H, Travaille C, Clucas C, Cooper A, et al.
1090 Extravascular Dermal Trypanosomes in Suspected and Confirmed Cases of
1091 *gambiense* Human African Trypanosomiasis. Clin Infect Dis. 2021;73(1):12-20. Epub
1092 2020/07/09. doi: 10.1093/cid/ciaa897. PubMed PMID: 32638003; PubMed Central
1093 PMCID: PMCPMC8246823.
1094 28. Bargul JL, Jung J, McOdimba FA, Omogo CO, Adung'a VO, Kruger T, et al.
1095 Species-Specific Adaptations of Trypanosome Morphology and Motility to the
1096 Mammalian Host. PLoS Pathog. 2016;12(2):e1005448. Epub 2016/02/13. doi:
1097 10.1371/journal.ppat.1005448. PubMed PMID: 26871910; PubMed Central PMCID:
1098 PMCPMC4752354.
1099 29. Sun SY, Kaelber JT, Chen M, Dong X, Nematbakhsh Y, Shi J, et al. Flagellum
1100 couples cell shape to motility in *Trypanosoma brucei*. Proc Natl Acad Sci U S A.
1101 2018;115(26):E5916-E25. Epub 2018/06/13. doi: 10.1073/pnas.1722618115. PubMed
1102 PMID: 29891682; PubMed Central PMCID: PMCPMC6042131.
1103 30. De Niz M, Bras D, Ouarne M, Pedro M, Nascimento AM, Henao Misikova L, et
1104 al. Organotypic endothelial adhesion molecules are key for *Trypanosoma brucei*
1105 tropism and virulence. Cell Rep. 2021;36(12):109741. Epub 2021/09/23. doi:
1106 10.1016/j.celrep.2021.109741. PubMed PMID: 34551286; PubMed Central PMCID:
1107 PMCPMC8480282.

1108 31. Shaw S, DeMarco SF, Rehmann R, Wenzler T, Florini F, Roditi I, et al. Flagellar
1109 cAMP signaling controls trypanosome progression through host tissues. Nat Commun.
1110 2019;10(1):803. Epub 2019/02/20. doi: 10.1038/s41467-019-08696-y. PubMed PMID:
1111 30778051; PubMed Central PMCID: PMCPMC6379439.
1112 32. Shaw S, Knusel S, Abbuhl D, Naguleswaran A, Etzensperger R, Benninger M,
1113 et al. Cyclic AMP signalling and glucose metabolism mediate pH taxis by African
1114 trypanosomes. Nat Commun. 2022;13(1):603. Epub 2022/02/03. doi: 10.1038/s41467-
1115 022-28293-w. PubMed PMID: 35105902; PubMed Central PMCID:
1116 PMCPMC8807625.
1117 33. Le Ray D, Barry JD, Easton C, Vickerman K. First tsetse fly transmission of the
1118 "AnTat" serodeme of *Trypanosoma brucei*. Ann Soc Belg Med Trop. 1977;57(4-5):369-
1119 81. Epub 1977/01/01. PubMed PMID: 610616.
1120 34. Bohringer S, Hecker H. Quantitative ultrastructural differences between strains
1121 of the *Tryponasoma brucei* subgroup during transformation in blood. J Protozool.
1122 1974;21(5):694-8. Epub 1974/11/01. doi: 10.1111/j.1550-7408.1974.tb03731.x.
1123 PubMed PMID: 4449091.
1124 35. Hirumi H, Hirumi K. Continuous cultivation of *Trypanosoma brucei* blood stream
1125 forms in a medium containing a low concentration of serum protein without feeder cell
1126 layers. J Parasitol. 1989;75(6):985-9. Epub 1989/12/01. PubMed PMID: 2614608.
1127 36. Barquilla A, Saldivia M, Diaz R, Bart JM, Vidal I, Calvo E, et al. Third target of
1128 rapamycin complex negatively regulates development of quiescence in *Trypanosoma*
1129 *brucei*. Proc Natl Acad Sci U S A. 2012;109(36):14399-404. doi:
1130 10.1073/pnas.1210465109. PubMed PMID: 22908264; PubMed Central PMCID:
1131 PMCPMC3437835.

1132 37. Czichos J, Nonnengaesser C, Overath P. *Trypanosoma brucei*: cis-aconitate
1133 and temperature reduction as triggers of synchronous transformation of bloodstream
1134 to procyclic trypomastigotes in vitro. Exp Parasitol. 1986;62(2):283-91. Epub
1135 1986/10/01. doi: 10.1016/0014-4894(86)90033-0. PubMed PMID: 3743718.
1136 38. Doyle JJ, Hirumi H, Hirumi K, Lupton EN, Cross GA. Antigenic variation in
1137 clones of animal-infective *Trypanosoma brucei* derived and maintained in vitro.
1138 Parasitology. 1980;80(2):359-69. Epub 1980/04/01. doi:
1139 10.1017/s0031182000000810. PubMed PMID: 6102753.
1140 39. Wang Z, Morris JC, Drew ME, Englund PT. Inhibition of *Trypanosoma brucei*
1141 gene expression by RNA interference using an integratable vector with opposing T7
1142 promoters. J Biol Chem. 2000;275(51):40174-9. Epub 2000/10/03. doi:
1143 10.1074/jbc.M008405200. PubMed PMID: 11013266.
1144 40. Wirtz E, Leal S, Ochatt C, Cross GA. A tightly regulated inducible expression
1145 system for conditional gene knock-outs and dominant-negative genetics in
1146 *Trypanosoma brucei*. Mol Biochem Parasitol. 1999;99(1):89-101. Epub 1999/04/24.
1147 PubMed PMID: 10215027.
1148 41. Redmond S, Vadivelu J, Field MC. RNAit: an automated web-based tool for the
1149 selection of RNAi targets in *Trypanosoma brucei*. Mol Biochem Parasitol.
1150 2003;128(1):115-8. Epub 2003/04/23. doi: 10.1016/s0166-6851(03)00045-8. PubMed
1151 PMID: 12706807.
1152 42. Burkard G, Fragoso CM, Roditi I. Highly efficient stable transformation of
1153 bloodstream forms of *Trypanosoma brucei*. Mol Biochem Parasitol. 2007;153(2):220-
1154 3. Epub 2007/04/06. doi: 10.1016/j.molbiopara.2007.02.008. PubMed PMID:
1155 17408766.

1156 43. Kelly S, Reed J, Kramer S, Ellis L, Webb H, Sunter J, et al. Functional genomics
1157 in *Trypanosoma brucei*: a collection of vectors for the expression of tagged proteins
1158 from endogenous and ectopic gene loci. Mol Biochem Parasitol. 2007;154(1):103-9.
1159 Epub 2007/05/22. doi: S0166-6851(07)00099-0 [pii]
1160 10.1016/j.molbiopara.2007.03.012. PubMed PMID: 17512617.
1161 44. Rotureau B, Ooi CP, Huet D, Perrot S, Bastin P. Forward motility is essential for
1162 trypanosome infection in the tsetse fly. Cell Microbiol. 2014;16(3):425-33. Epub
1163 2013/10/19. doi: 10.1111/cmi.12230. PubMed PMID: 24134537.
1164 45. Dacheux D, Landrein N, Thonnus M, Gilbert G, Sahin A, Wodrich H, et al. A
1165 MAP6-related protein is present in protozoa and is involved in flagellum motility. PLoS
1166 One. 2012;7(2):e31344. Epub 2012/02/23. doi: 10.1371/journal.pone.0031344.
1167 PubMed PMID: 22355359; PubMed Central PMCID: PMCPMC3280300.
1168 46. Dean S, Marchetti R, Kirk K, Matthews KR. A surface transporter family conveys
1169 the trypanosome differentiation signal. Nature. 2009;459(7244):213-7. Epub
1170 2009/05/16. doi: nature07997 [pii]
1171 10.1038/nature07997. PubMed PMID: 19444208.
1172

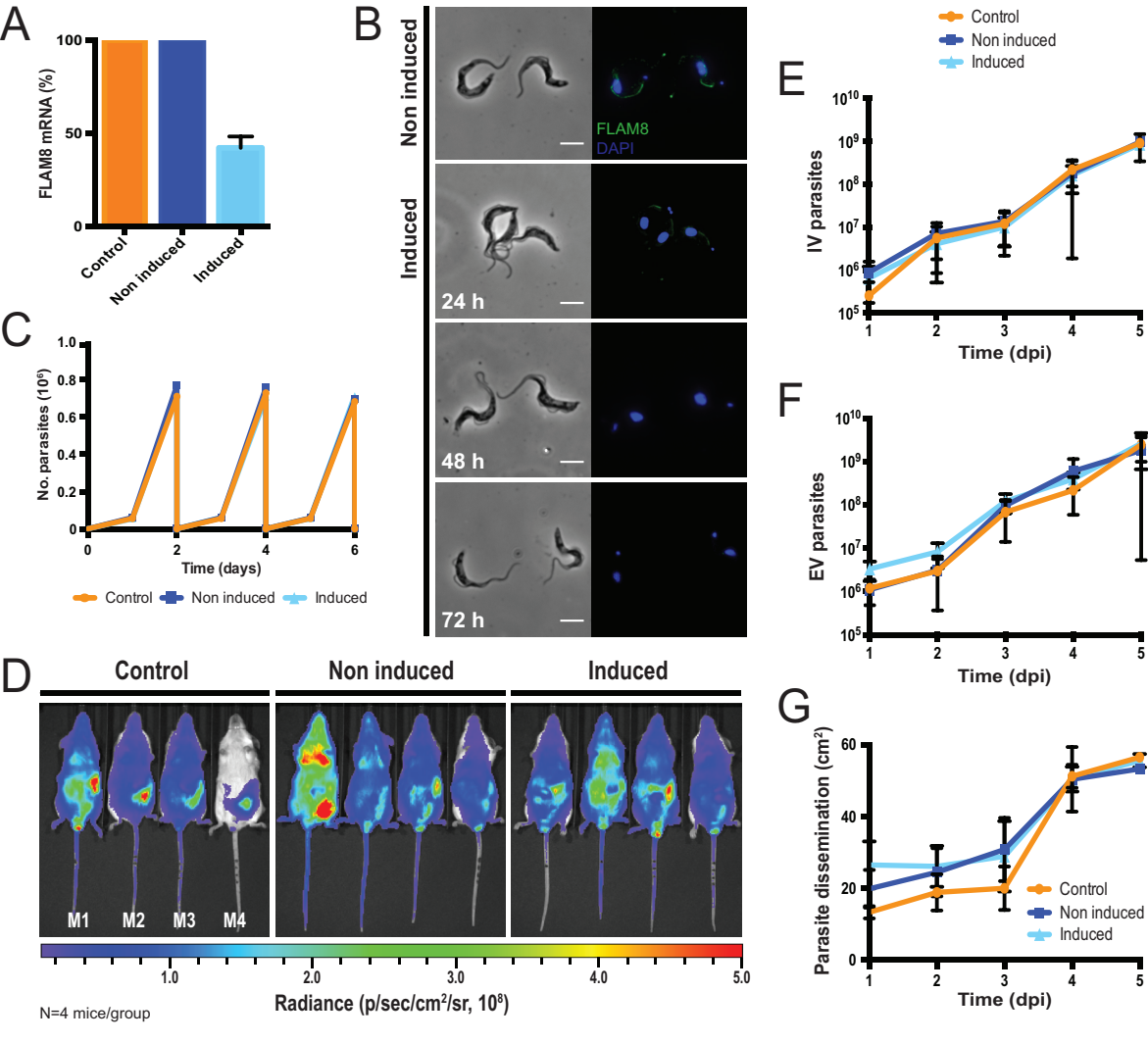
A
FLAM8 mRNA (%)
100
50
0
Control
Non induced
Induced
B
Non induced
Induced
FLAM8
DAPI
24 h
48 h
72 h
C
No. parasites (10^6)
1.0
0.8
0.6
0.4
0.2
0
0
2
4
6
Time (days)
Control
Non induced
Induced
D
Control
Non induced
Induced
M1
M2
M3
M4
1.0
2.0
3.0
4.0
5.0
Radiance (p/sec/cm²/sr, 10⁸)
N=4 mice/group
E
Control
Non induced
Induced
IV parasites
10^10
10^9
10^8
10^7
10^6
10^5
1
2
3
4
5
Time (dpi)
F
EV parasites
10^10
10^9
10^8
10^7
10^6
10^5
1
2
3
4
5
Time (dpi)
G
Parasite dissemination (cm²)
60
40
20
0
Control
Non induced
Induced
1
2
3
4
5
Time (dpi)

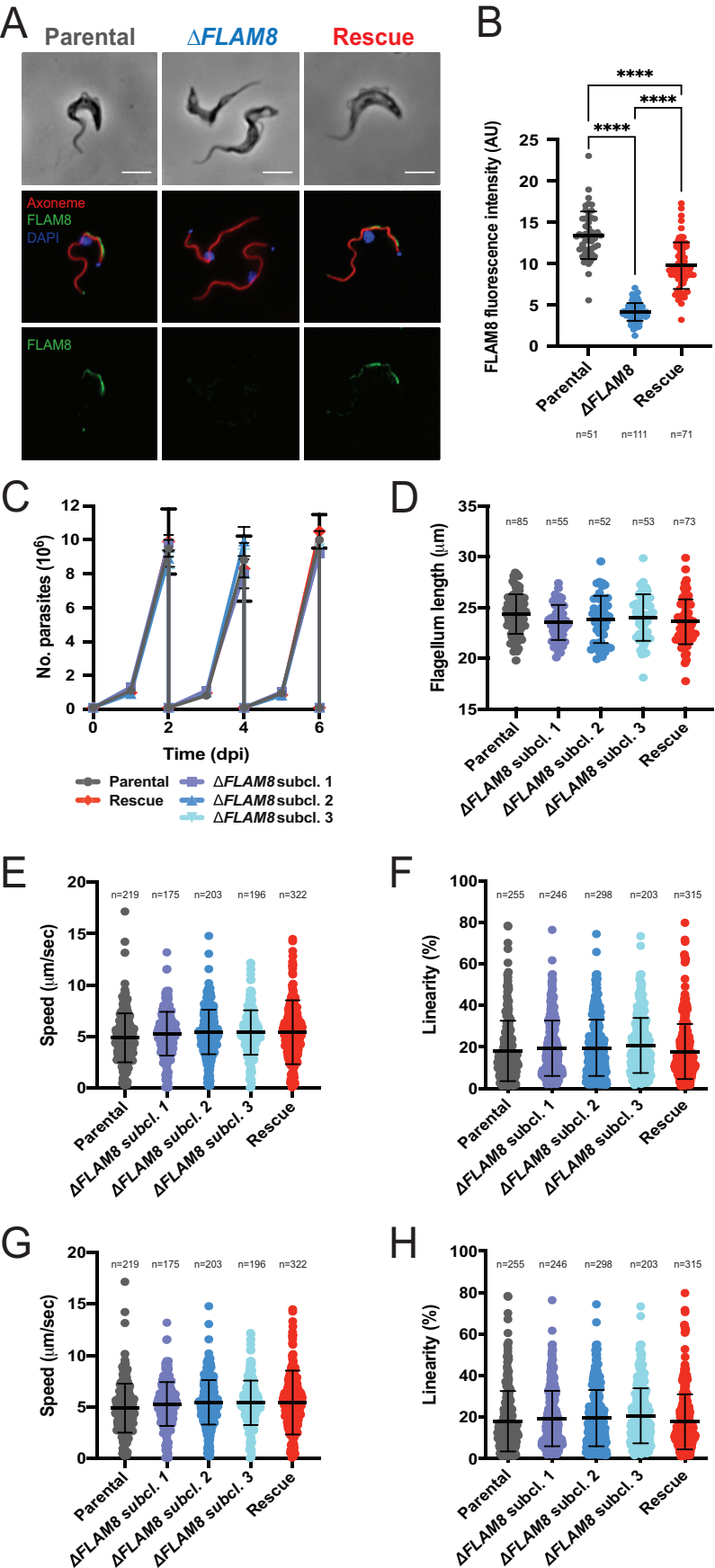
A
Parental
ΔFLAM8
Rescue
Axoneme
FLAM8
DAPI
FLAM8
B
FLAM8 fluorescence intensity (AU)
****
****
****
Parental
ΔFLAM8
Rescue
n=51
n=111
n=71
C
No. parasites (10^6)
Time (dpi)
Parental
Rescue
ΔFLAM8 subcl. 1
ΔFLAM8 subcl. 2
ΔFLAM8 subcl. 3
D
Flagellum length (µm)
n=85
n=55
n=52
n=53
n=73
Parental
ΔFLAM8 subcl. 1
ΔFLAM8 subcl. 2
ΔFLAM8 subcl. 3
Rescue
E
Speed (µm/sec)
n=219
n=175
n=203
n=196
n=322
F
Linearity (%)
n=255
n=246
n=298
n=203
n=315
G
Speed (µm/sec)
n=219
n=175
n=203
n=196
n=322
H
Linearity (%)
n=255
n=246
n=298
n=203
n=315

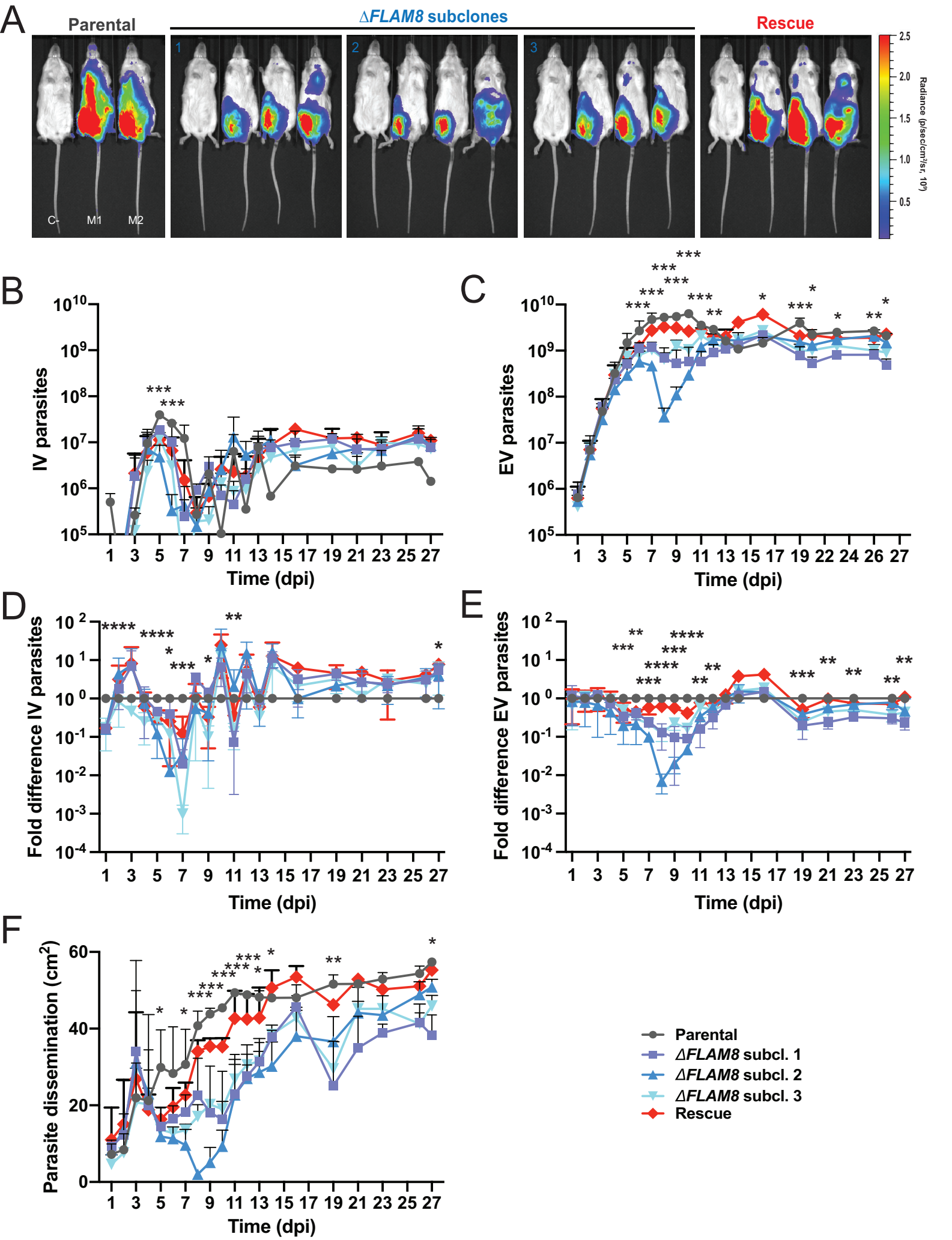
A
Parental
ΔFLAM8 subclones
Rescue
1
2
3
C-
M1
M2
Radiance (p/sec/cm²/sr, 10⁶)
B
IV parasites
Time (dpi)
C
EV parasites
Time (dpi)
D
Fold difference IV parasites
Time (dpi)
E
Fold difference EV parasites
Time (dpi)
F
Parasite dissemination (cm²)
Time (dpi)
Parental
ΔFLAM8 subcl. 1
ΔFLAM8 subcl. 2
ΔFLAM8 subcl. 3
Rescue

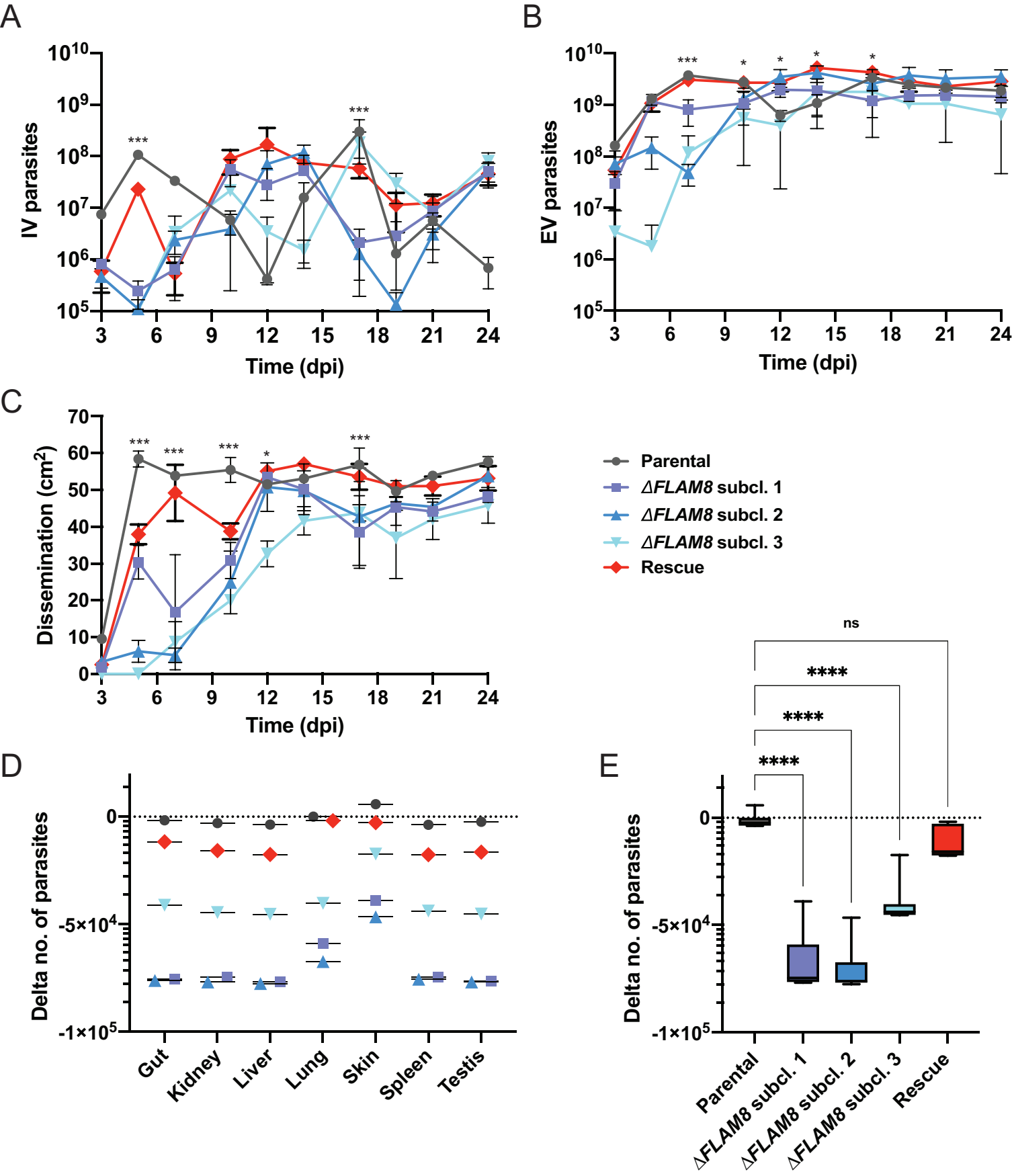
A
IV parasites
Time (dpi)
B
EV parasites
Time (dpi)
C
Dissemination (cm²)
Time (dpi)
Parental
ΔFLAM8 subcl. 1
ΔFLAM8 subcl. 2
ΔFLAM8 subcl. 3
Rescue
D
Delta no. of parasites
Gut
Kidney
Liver
Lung
Skin
Spleen
Testis
E
Delta no. of parasites
ns
****
Parental
ΔFLAM8 subcl. 1
ΔFLAM8 subcl. 2
ΔFLAM8 subcl. 3
Rescue

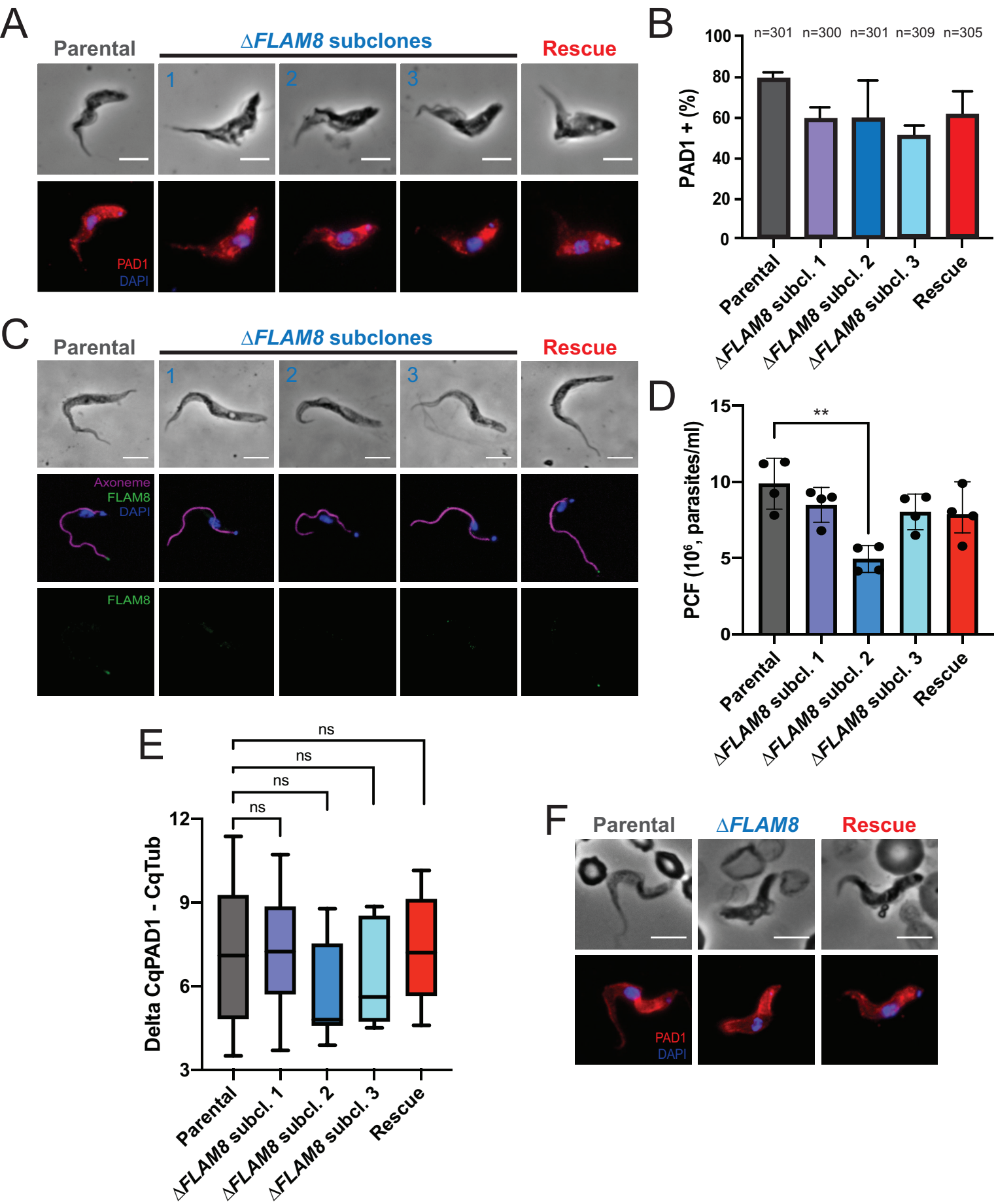
A
Parental
ΔFLAM8 subclones
Rescue
1
2
3
PAD1
DAPI
B
n=301 n=300 n=301 n=309 n=305
PAD1 + (%)
100
80
60
40
20
0
Parental
ΔFLAM8 subcl. 1
ΔFLAM8 subcl. 2
ΔFLAM8 subcl. 3
Rescue
C
Parental
ΔFLAM8 subclones
Rescue
1
2
3
Axoneme
FLAM8
DAPI
FLAM8
D
PCF (10^6, parasites/ml)
15
10
5
0
**
Parental
ΔFLAM8 subcl. 1
ΔFLAM8 subcl. 2
ΔFLAM8 subcl. 3
Rescue
E
ns
ns
ns
ns
Delta CqPAD1 - CqTub
12
9
6
3
Parental
ΔFLAM8 subcl. 1
ΔFLAM8 subcl. 2
ΔFLAM8 subcl. 3
Rescue
F
Parental
ΔFLAM8
Rescue
PAD1
DAPI

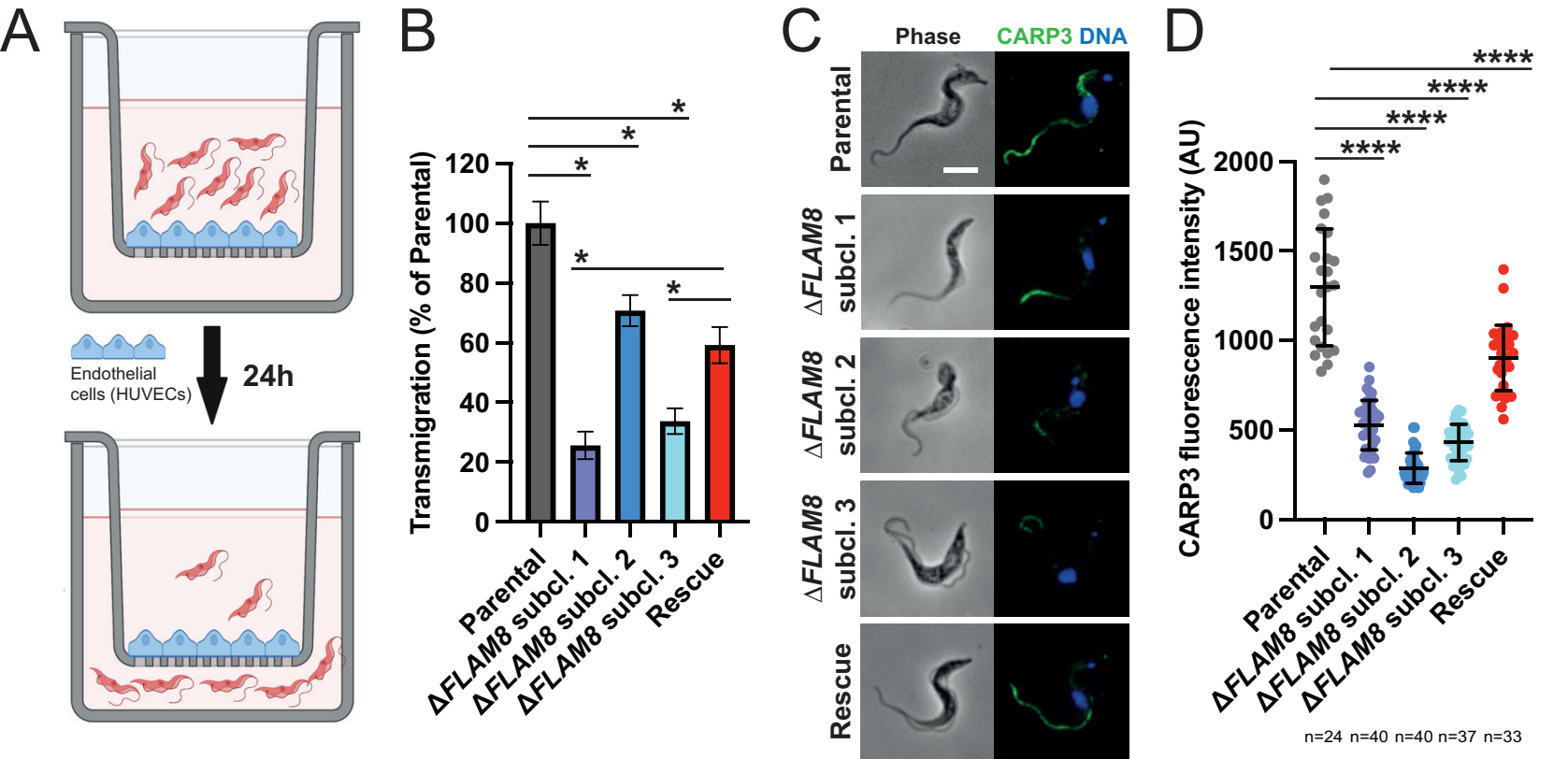
A
Endothelial cells (HUVECs)
24h
B
Transmigration (% of Parental)
120
100
80
60
40
20
0
*
*
*
*
*
Parental
ΔFLAM8 subcl. 1
ΔFLAM8 subcl. 2
ΔFLAM8 subcl. 3
Rescue
C
Phase
CARP3 DNA
Parental
ΔFLAM8 subcl. 1
ΔFLAM8 subcl. 2
ΔFLAM8 subcl. 3
Rescue
D
CARP3 fluorescence intensity (AU)
2000
1500
1000
500
0
****
****
****
****
Parental
ΔFLAM8 subcl. 1
ΔFLAM8 subcl. 2
ΔFLAM8 subcl. 3
Rescue
n=24 n=40 n=40 n=37 n=33

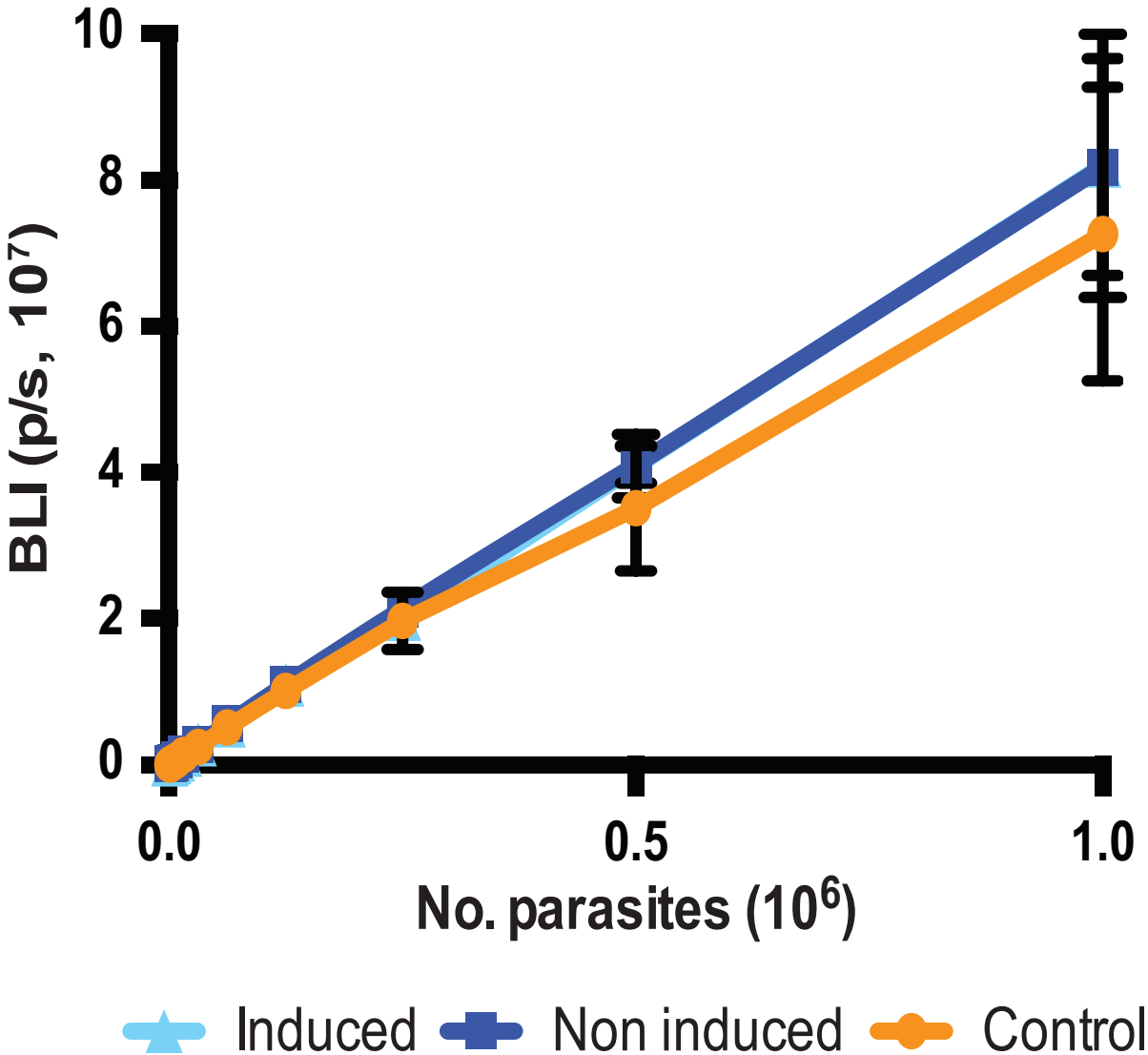
BLI (p/s, 10^7)
10
8
6
4
2
0
0.0
0.5
1.0
No. parasites (10^6)
Induced
Non induced
Control

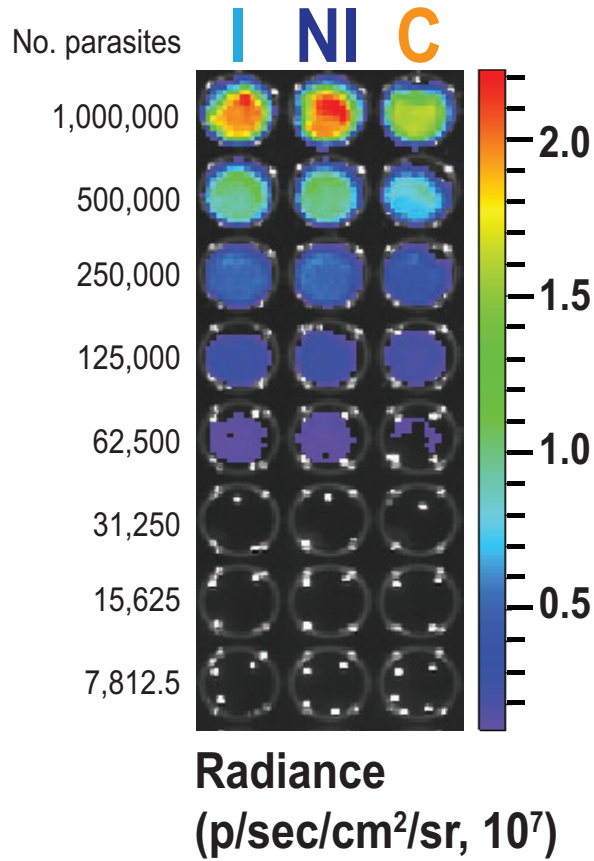
No. parasites
I
NI
C
1,000,000
500,000
250,000
125,000
62,500
31,250
15,625
7,812.5
2.0
1.5
1.0
0.5
Radiance
(p/sec/cm²/sr, 10⁷)

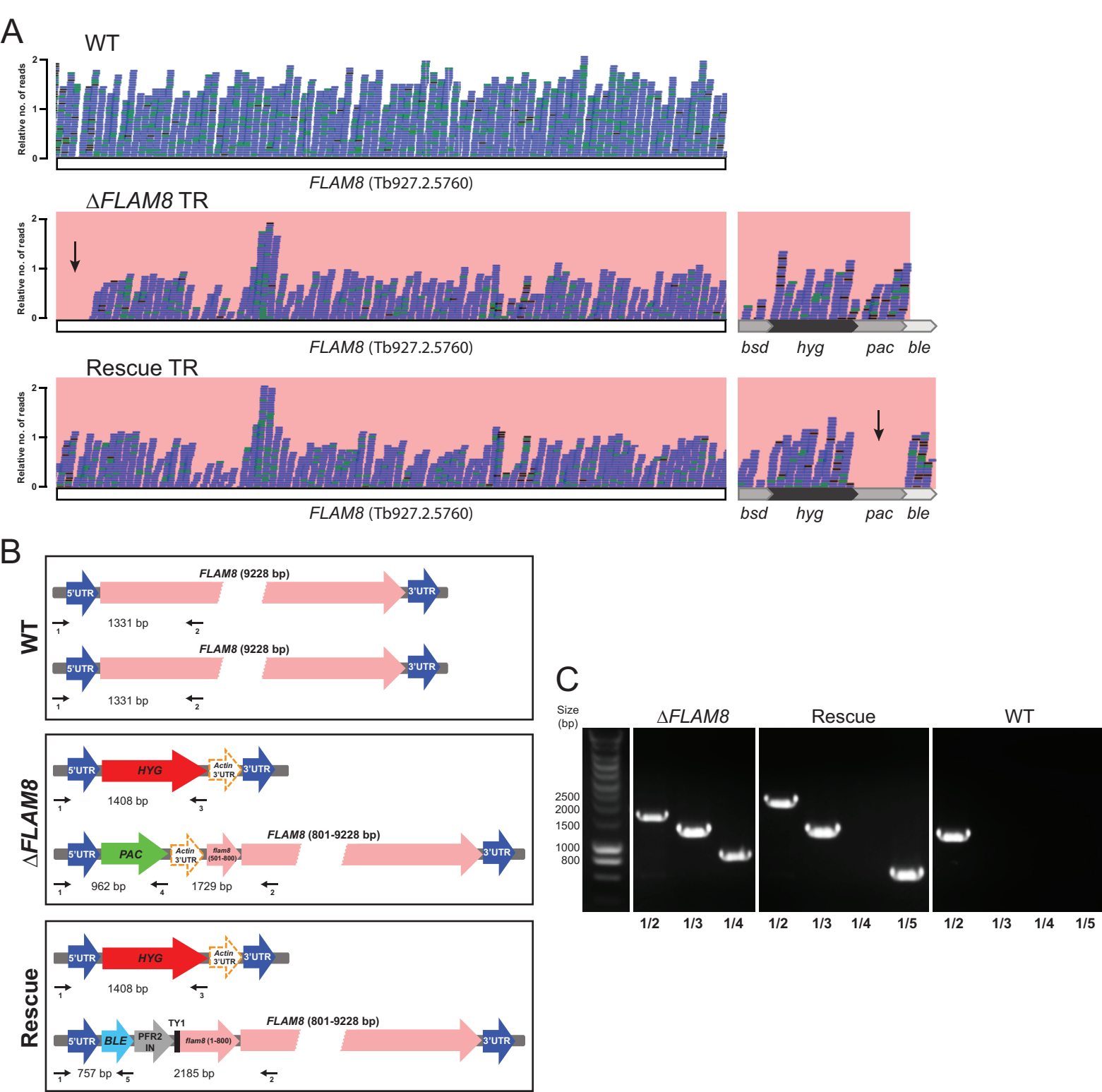
A
WT
Relative no. of reads
FLAM8 (Tb927.2.5760)
ΔFLAM8 TR
bsd
hyg
pac
ble
Rescue TR
B
WT
FLAM8 (9228 bp)
5'UTR
3'UTR
1331 bp
ΔFLAM8
HYG
Actin 3'UTR
1408 bp
PAC
flam8 (501-800)
FLAM8 (801-9228 bp)
962 bp
1729 bp
Rescue
BLE
PFR2 IN
TY1
flam8 (1-800)
757 bp
2185 bp
C
Size (bp)
ΔFLAM8
Rescue
WT
2500
2000
1500
1000
800
1/2
1/3
1/4
1/5

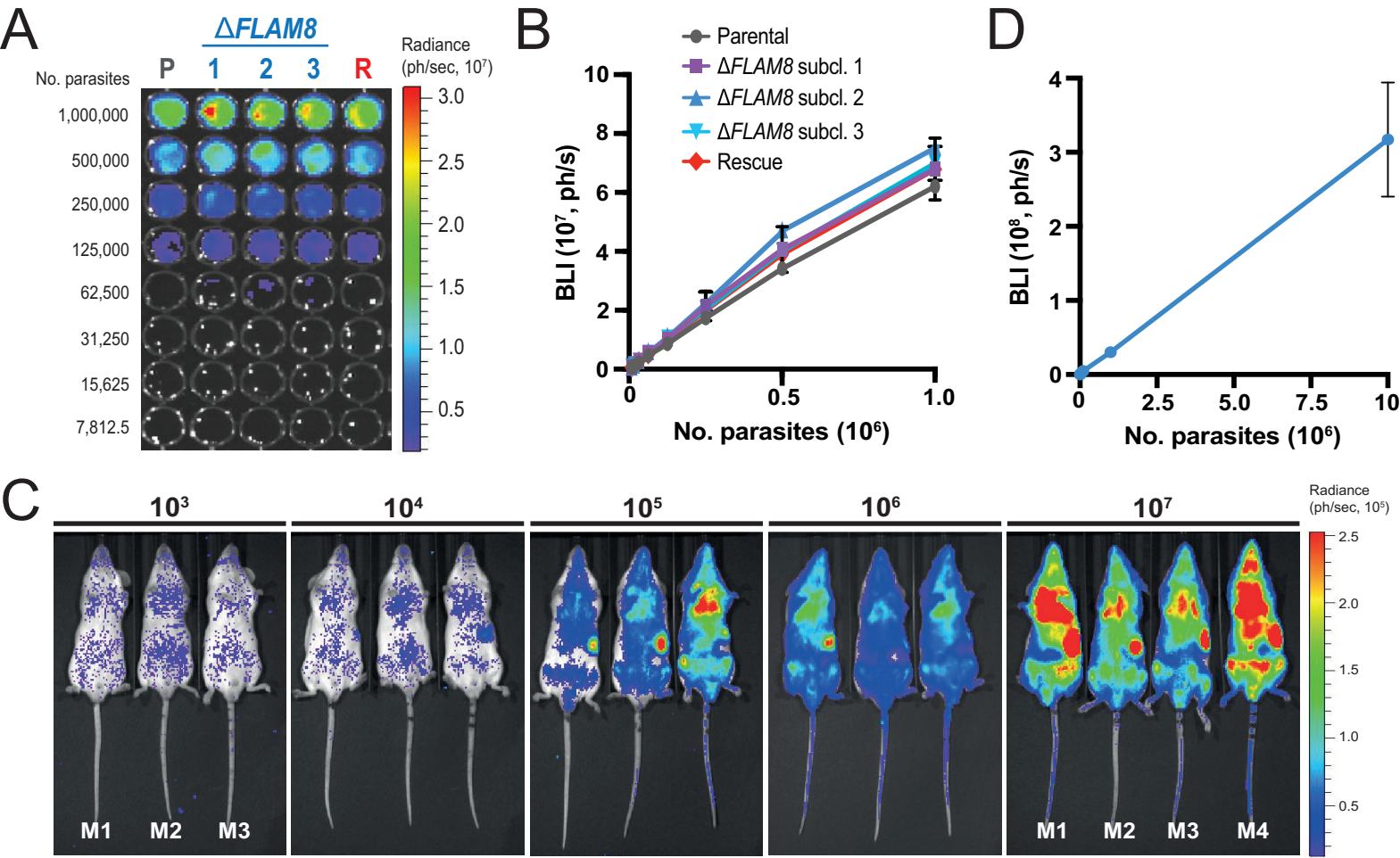
A
ΔFLAM8
P
1
2
3
R
No. parasites
1,000,000
500,000
250,000
125,000
62,500
31,250
15,625
7,812.5
Radiance (ph/sec, 10⁷)
3.0
2.5
2.0
1.5
1.0
0.5
B
Parental
ΔFLAM8 subcl. 1
ΔFLAM8 subcl. 2
ΔFLAM8 subcl. 3
Rescue
BLI (10⁷, ph/s)
No. parasites (10⁶)
D
BLI (10⁸, ph/s)
No. parasites (10⁶)
C
10³
10⁴
10⁵
10⁶
10⁷
Radiance (ph/sec, 10⁵)
M1
M2
M3
M4

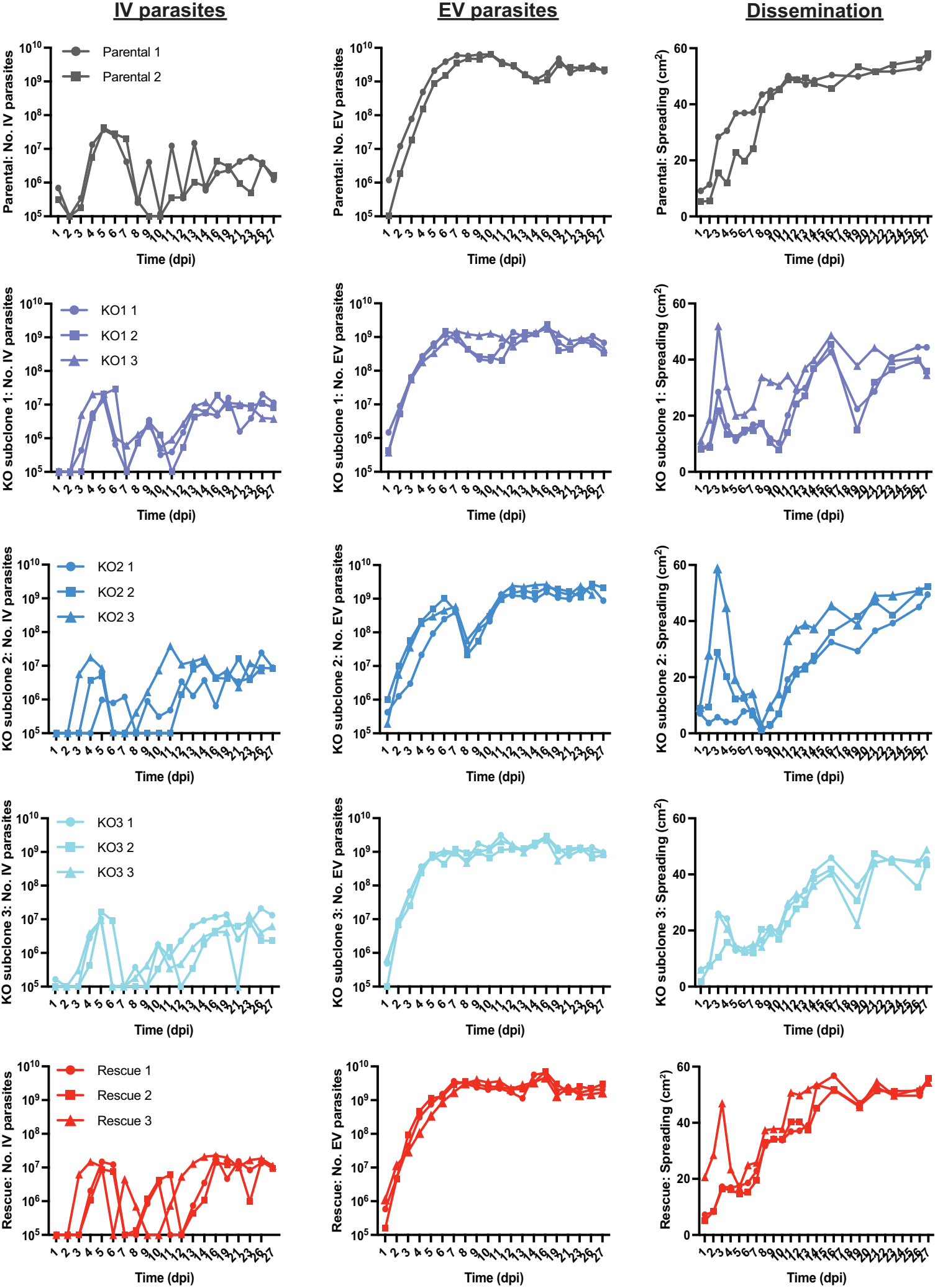
IV parasites
EV parasites
Dissemination
Parental 1
Parental 2
Parental: No. IV parasites
Parental: No. EV parasites
Parental: Spreading (cm²)
KO1 1
KO1 2
KO1 3
KO subclone 1: No. IV parasites
KO subclone 1: No. EV parasites
KO subclone 1: Spreading (cm²)
KO2 1
KO2 2
KO2 3
KO subclone 2: No. IV parasites
KO subclone 2: No. EV parasites
KO subclone 2: Spreading (cm²)
KO3 1
KO3 2
KO3 3
KO subclone 3: No. IV parasites
KO subclone 3: No. EV parasites
KO subclone 3: Spreading (cm²)
Rescue 1
Rescue 2
Rescue 3
Rescue: No. IV parasites
Rescue: No. EV parasites
Rescue: Spreading (cm²)
Time (dpi)

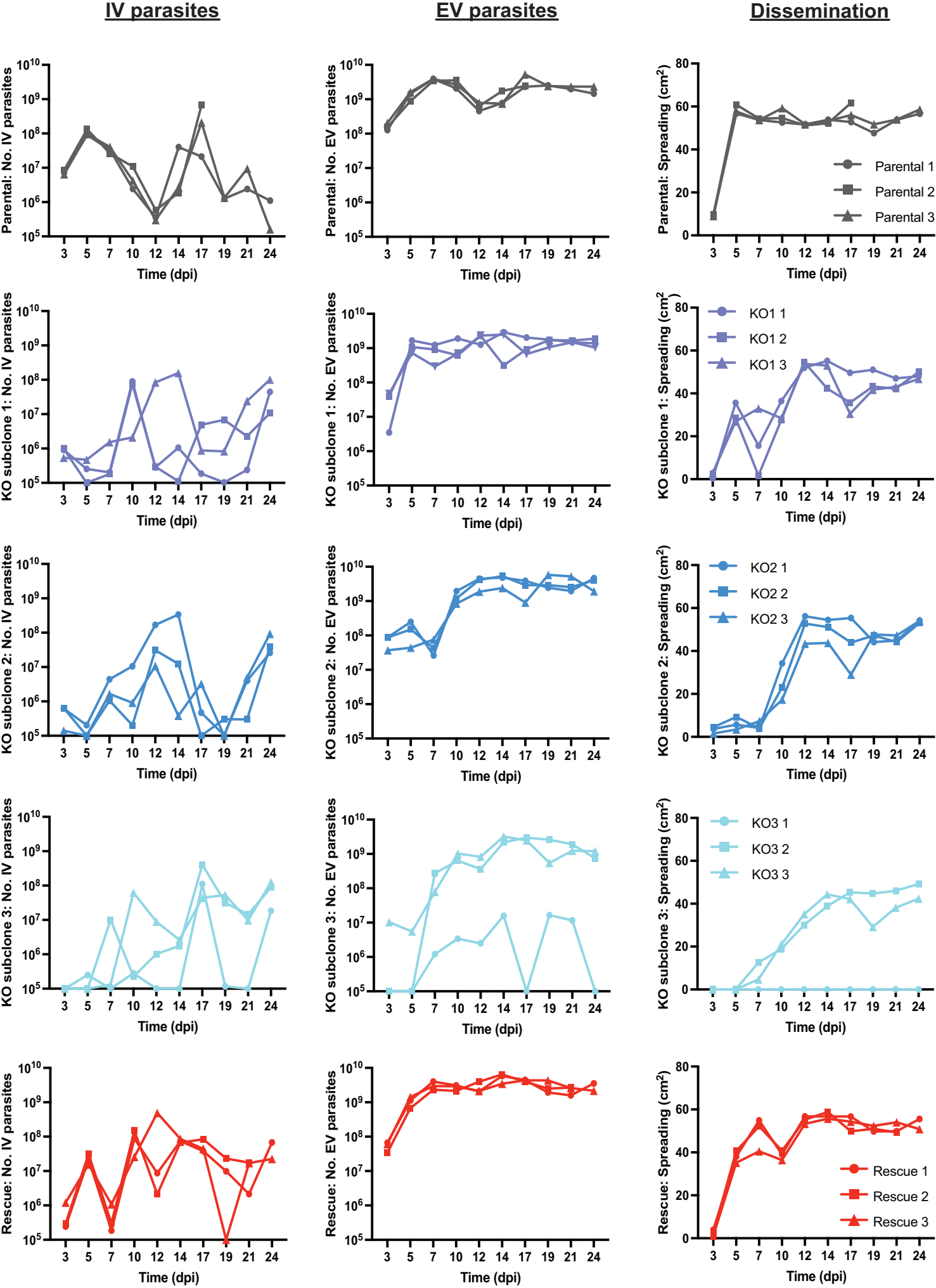
IV parasites
EV parasites
Dissemination
Parental: No. IV parasites
Parental: No. EV parasites
Parental: Spreading (cm²)
Parental 1
Parental 2
Parental 3
KO subclone 1: No. IV parasites
KO subclone 1: No. EV parasites
KO subclone 1: Spreading (cm²)
KO1 1
KO1 2
KO1 3
KO subclone 2: No. IV parasites
KO subclone 2: No. EV parasites
KO subclone 2: Spreading (cm²)
KO2 1
KO2 2
KO2 3
KO subclone 3: No. IV parasites
KO subclone 3: No. EV parasites
KO subclone 3: Spreading (cm²)
KO3 1
KO3 2
KO3 3
Rescue: No. IV parasites
Rescue: No. EV parasites
Rescue: Spreading (cm²)
Rescue 1
Rescue 2
Rescue 3
Time (dpi)
3 5 7 10 12 14 17 19 21 24
10^{5} 10^{6} 10^{7} 10^{8} 10^{9} 10^{10}
0 20 40 60 80

A

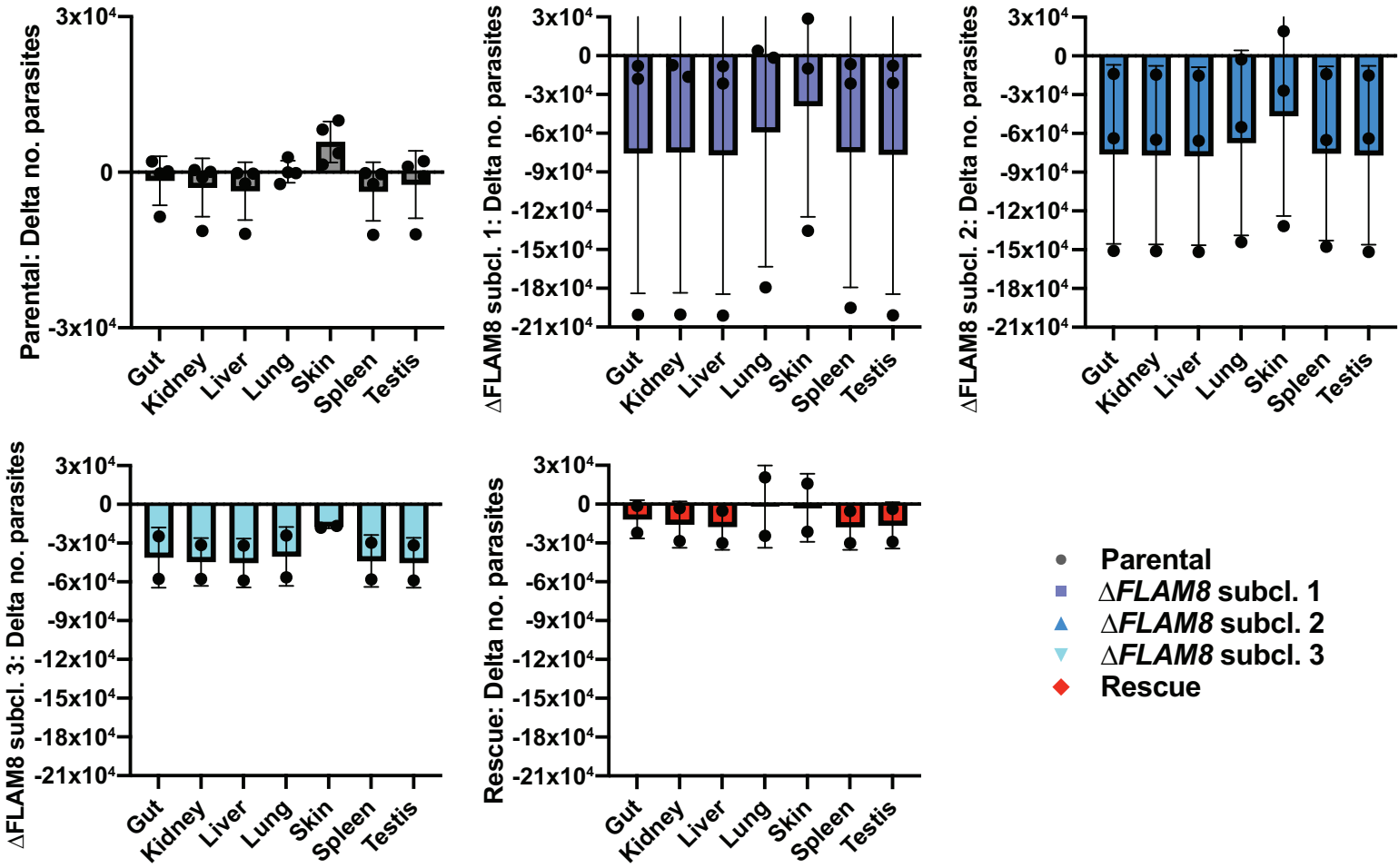
Parental: Delta no. parasites
ΔFLAM8 subcl. 1: Delta no. parasites
ΔFLAM8 subcl. 2: Delta no. parasites
ΔFLAM8 subcl. 3: Delta no. parasites
Rescue: Delta no. parasites
3x10⁴
0
-3x10⁴
-6x10⁴
-9x10⁴
-12x10⁴
-15x10⁴
-18x10⁴
-21x10⁴
Gut
Kidney
Liver
Lung
Skin
Spleen
Testis
Parental
ΔFLAM8 subcl. 1
ΔFLAM8 subcl. 2
ΔFLAM8 subcl. 3
Rescue

B

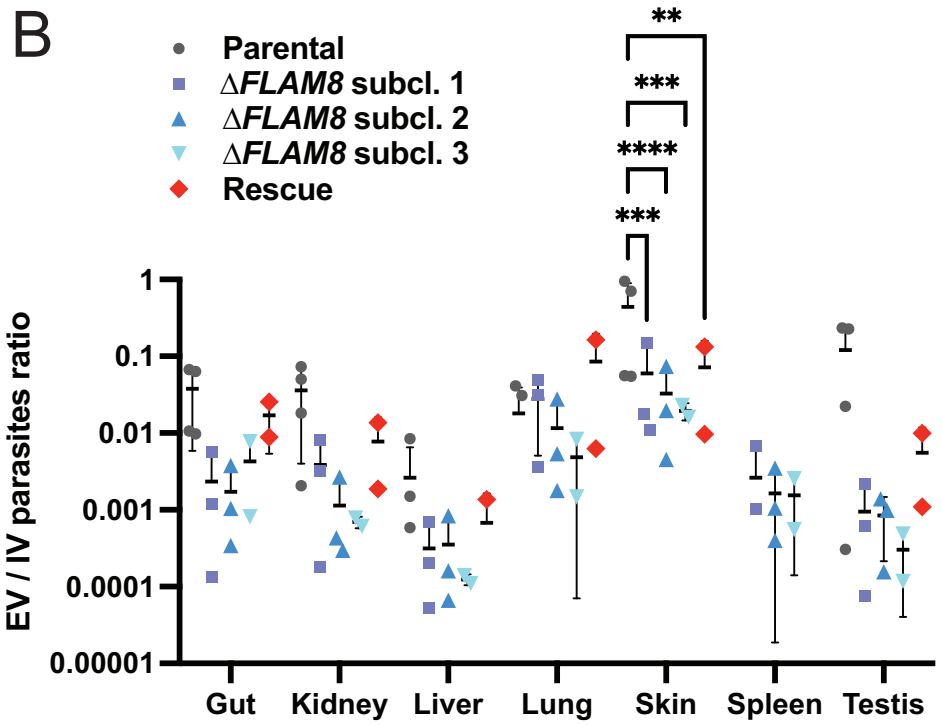
Parental
ΔFLAM8 subcl. 1
ΔFLAM8 subcl. 2
ΔFLAM8 subcl. 3
Rescue
**
***
****
***
EV / IV parasites ratio
1
0.1
0.01
0.001
0.0001
0.00001
Gut
Kidney
Liver
Lung
Skin
Spleen
Testis